TÉCNICO LISBOA

Numerical simulation of a thermoelectric generator module for road vehicles

Piotr Franciszek Raczkowski

Thesis to obtain the Master of Science Degree in

Energy Engineering and Management

Supervisor: Prof. Pedro Jorge Martins Coelho

Examination Committee

Chairperson: Prof. Edgar Caetano Fernandes

Supervisor: Prof. Pedro Jorge Martins Coelho

Member of the Committee: Prof. José Maria Campos da Silva André

January 2021

Acknowledgments

I want to acknowledge Dr Karol Sztekler - supervisor from the side of AGH University of Science and Technology in Krakow. The thesis was elaborated under the InnoEnergy Master School Programme.

Abstract

Nowadays, almost every industry sector in Europe is facing the impose of strict rules regarding energy savings in order to reduce emissions of greenhouse gases. The regulations, encourage industries to constantly look for improvements. Now, the automotive industry is looking for a every possible manner of upgrade allowing to improve cars efficiency. One of the possible solution is to install thermoelectric generators to reuse the waste heat released with fumes. To investigate whether TEGs implementation could be a good manner to improve the efficiency there is a need to mathematically model the device in order to check its performance. The presented thesis focus on elaboration of benchmark procedure for thermoelectric numerical modelling in ANSYS Workbench using Thermal-Electric module. In the introductory part of the thesis one can find the literature survey in the topic of TEGs modeling, the physical fundamentals of thermoelectric along with modelling procedure explained. Then the mathematical model implementation in ANSYS is described. The following part contains the results description and analysis. In the last chapter the final conclusions and future plans are presented.

Keywords: Thermoelectric generator, Numerical modeling, ANSYS Workbench, Contact Resistances, HZ-14

Contents

List of Tables

List of Figures

Nomenclature

Roman and greek symbols

A	area	[m^2]
C	specific heat capacity	[J/kg K]
I	current	[A]
$\dot{J}$	volumetric current density	[J/m^3]
k	thermal conductivity	[W/m K]
$\dot{Q}$	heat power	[W]
$\dot{q}$	heat generation per unit volume	[W/m^3]
q	heat flux vector	[W/m^2]
R	internal resistance	[Ohm]
R_{load}	load resistance	[Ohm]
T	temperature	[K]
V	potential difference	[V]
W	power	[W]
Z	figure of merit	[-]

α	Seebeck coefficient	[V/K]
δ	difference	[-]
η	electrical efficiency	[-]
ρ	material electric resistivity	[Ohm m]
ρ	density	[kg/m^3]
κ	Thomson coefficient	[V/K]
ϕ	electric potential	[V]
Π	Peltier coefficient	[J/C]

Subscripts

c	cold
h	hot
J	Joule
T	transpose

Abreviations

CFD	Computational Fluid Dynamics
ETEG	Exhaust-Based Thermoelectric Generators
FEM	Finite Element Method
FVM	Finite Volume Method
HZ-14	Commercial thermoelectric module manufactured by $Hi-Z\ Technology$
ICE	Internal Combustion Engine
TEG	Thermoelectric Generator

Model explanation

1st model	basic model containing constant value of material properties
2nd model	model containing non-linear temperature dependent material properties
3rd model	full model containing non-linear temperature dependent material properties and contact resistances applied

Chapter 1

Introduction

In the era of sustainable development we currently live in, the energy revolution is taking place on our planet. Today, not only the amount of energy produced is a priority but the methods it is obtained with. This revolution is not only limited to the energy sector but affects different industries such as construction or automotive. Broadly understood power sources are expected to affect the environment as little as possible. This is very evident in the automotive industry, where either electric or hybrid solutions are implemented to maximize engine efficiency and reduce emissions. One of the devices that are used to improve the efficiency of internal combustion engines is a thermoelectric generator that uses low-quality waste heat to convert it to useful electricity using the Seebeck phenomenon.

1.1 Motivation

Year by year international institutions like the European Union impose more strict rules on the automotive sector, having a purpose to reduce the global emission of greenhouse gases. In order to maintain its leadership, Europe established an averaged CO_2 emission target for car manufacturers fleet at the level of 95 g per km till 2020. [1] Although there is a big pressure on the automotive industry, until 2035 the oil-fueled transport is expected to maintain its leadership on the market at the level of 89 % [2]. This is provoked mainly by the elevated price of batteries or fuel cell systems. Internal combustion engines (ICE) are the cheapest drive for cars and this trend is expected to maintain in the coming years.

Current car efficiency is around 25 % under typical driving conditions [3] and the remaining is wasted as heat. The abovementioned facts force manufacturers to increase the engine system efficiency via the implementation of different upgrades like turbochargers, exhaust gas recirculation, or thermoelectric generators. Unfortunately, ICEs do not convert chemical energy efficiently to useful mechanical energy, because of the dissipation of energy in exhaust and coolant. That is why, currently the improvements are made in an indirect way, trying to recover the waste heat.[4] Although the internal combustion engine efficiency is limited by the Carnot rule, its efficiency can still be increased through the recuperation of energy carried by exhaust gases. This could help to boost the efficiency of these engines considerably and help the classic powertrain to fulfill severe norms. One of the technologies which are being developed in

the area is TEG. This type of waste recovery system allows to convert the remaining heat into electricity reducing the alternator load. Thereby it diminishes fuel consumption which leads to reduced emission of CO_2. Thermoelectric generators and heat pipes are a good solution to enhance ICEs performance. They are just simple solid-state devices without any moving parts and additional equipment. Thanks to their light weighted, compact size and simplicity in operation they are an ideal solution to recover waste heat in automotive application.[4] The TEG usefulness is not only limited to automotive applications. This technology has many potential applications in industry as a waste heat recovery system for low-quality heat or micro-generation for sensors and microelectronics.[5]

1.2 Literature Survey

Waste heat management is an important issue in the majority of industries because it has the potential to make processes or devices more economic. Among different manners to do that thermoelectricity is starting to take off. Thermoelectric systems are composed of a series of thermoelectric modules(consisted of hundreds of thermocouples) placed between two heat exchangers. The simplicity of their construction, direct conversion mechanism, a long lifespan in stable heat conditions, no maintenance cost, and noiseless operation make them a promising remedy for saving energy. Despite having a list of advantages, so far TEGs application was limited to microelectronics and space application, mainly because of its low efficiency and relatively large costs. [5]

Nowadays researchers focus on improving thermoelectrics in three main areas, which are: enhance $\mathcal{Z}T$ -material property, expand the operating temperature range for specific materials and decrease the manufacturing cost, or discover low-cost materials to balance the low efficiency. Despite TEGs low efficiency, the high reliability and no maintenance characteristics favor thermoelectric systems in remote areas, where power availability is a critical issue. In places like offshore platforms, well sites, telecommunication stations in mountains, or deserts TEGs combined with gas burners are used. Furthermore, they are a suitable solution to supply microelectronics and sensors, which require only milliwatts of power. In many cases it is easier to assemble them along with thermoelectric module installed on some heat source like hot pipes, steam lines, etc. instead of fixing long wires to grid source.[5]

Currently, the available TEG systems have system efficiency around 5 % which is not enough for the majority of industrial applications, but thanks to the before-mentioned wide range of advantages it can be applied in numerous specific appliances. One of the most promising fields where thermoelectric modules started to get attention is the automotive industry. Big companies like Renault, BMW, Ford, General Motors, and Scania have revealed their interest in exhaust gas recovery systems supported with TEGs. The technology has not been installed in a commercial vehicle yet, but there are researches carried out within the topic.[4] For a car application exhaust based thermoelectric generators (ETEG) are placed at the exhaust pipe. The hot side is heated by the exhaust gases and the other side is cooled by the engine coolant. Thermoelectric modules are placed on the surface of heat exchangers which can have a rectangular or hexagonal shape. The examples of ETEG are shown in the figures below:

The studies in the area of thermoelectricity application in the automotive sector distinguish into two

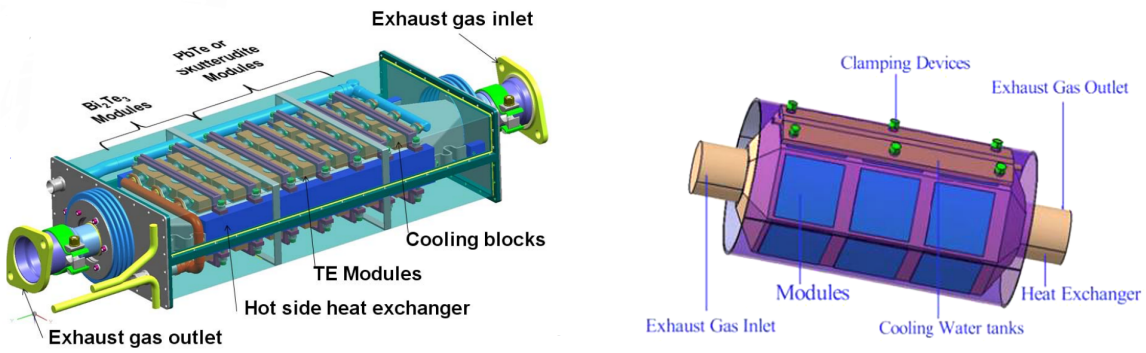

(a) rectangular shaped ETEG - General Motors.[6]

(b) hexagonal-prism shaped ETEG[7]

Figure 1.1: Examples of ETEG system design.

main blocks: experimental analysis and numerical modeling. The first approach is intuitive and gives us direct information regarding the performance of the studied device although it is very expensive, time-consuming, and has a reduced potential to induce some sort of speculation. Nowadays in modern engineering, mathematical modeling gets enormous attention in multiple applications. Thanks to increasing computer power we can study various processes with minimum financial resources. It allows us to ask multiple questions simultaneously and learn the way we should follow. Obviously, the mathematical model should be validated with an experiment reviewing its performance, but when successfully passed, then it can be used to perform some parametric study when looking for other improvements in the examined phenomenon.

This thesis focus on the modeling aspect in the area of thermoelectric generator application for road vehicles. In the literature, one can find different models of TEGs which differ between each other in dimensionality, numerical schemes, and assumptions. Zhang[8] has proposed a 1D model describing the HZ-14 commercial TEG module, where he obtained a nonlinear analytical solution for the transport equation, taking into consideration the temperature dependence of material properties. In [9] there is also an analytical model proposed and validated with experimental data for different operating conditions. Although analytical models are the best alternatives, the complexity of the phenomenon forces researches to develop numerical models that can handle multi-dimensional modeling and condition-dependent material properties. The 3D numerical models are in advantage. Niu at al. [10] elaborated two 3D models using FVM where the different solving procedure of conservation equation was implemented. Additionally, the impact of thermolectric legs shape on efficiency was investigated, showing that properly shaped hexahedronal legs can enhance the temperature gradient. Some of the studies focus on directly practical aspects of the TEG application. In [11] one can find a 3D model build with Finite Element Method showing that it is hard to provide significant fuel savings with ETEG application even if the assembly is well-suited. Similar considerations were observed in [12] where it is shown that in heavy-duty vehicles with ETEG only 2% of exhaust gases heat can be recovered and converted to electrical power. Moreover, they underline that the thermoelectric design, especially couples design plays a significant role in electrical power output. So as we can see there is still a lot to do within the topic.

The abovementioned models are steady-state, but one can also find dynamic models [13], where it

is proven for TEGs that due to much faster electric response than thermal, power output is synchronous to the load current and it has a relatively fast response to exhaust gas physical properties only limited by the thermal diffusion.

More detailed publications like [14] and [15] contain a full numerical 3-dimensional description of exhaust-based thermoelectric generators (ETEG) with nonlinear-fluid-thermal-electric multiphysics coupled simulation and having temperature-dependent characteristics of materials included. These models are based on a finite-volume scheme built with the help of ANSYS FLUENT. They claim that ETEG geometry has to be designed for specific engines, respecting its operating condition in order to allow the thermoelectric generator to operate efficiently.

1.3 Objectives

Knowing the current state of the art in thermoelectric generators modeling it is important to know that there is still a lot of research needed in the area of thermoelectric modeling in order to know what parameters are essential for its operation. The focus of the thesis is to model a real thermoelectric module using a 3D numerical code and check the influence of different modeling approaches. One of the key features of the model is to implement non-linear, temperature-dependent physical parameters of p-type and n-type material and contact resistances between legs and couples and examine its influence on the model performance. The aim is to obtain a detailed, well-described numerical model combined with suitable boundary conditions in order to get an appropriate benchmark for modeling thermoelectric generators.

1.4 Thesis Outline

The second chapter is dedicated to the physical description of the thermoelectricity phenomenon with an explanation of how elementary properties influence its performance. The TEGs operations rules are attached. It also contains the most important equations and the mathematical model is clarified. The third chapter describes the mathematical model implementation. It consists of the description of the studied device; thermoelectric generator HZ-14[16] and its properties, the description of the numerical model with numerical method incorporated and numerical scheme explained. In the fourth chapter, one can find a detailed analysis of obtained numerical results with a comparison of different modeling scenarios and comparision with experimental data for a real thermoelectric module. Moreover, the outcome of the calculations is discussed. The last chapter focuses on the model evaluation; the most important conclusions and the possible improvements which can be introduced to the model in the future.

Chapter 2

Thermoelectric generators: fundamentals and modeling

Thermoelectric generators are a group of devices that are able to directly convert thermal energy into electrical energy. The phenomenon is based on an electric potential generated between p-type and n-type semiconductors as a result of temperature difference. TEG, thanks to its advantages like no moving parts, no fuel consumption, and compact design can be used to recover waste heat in internal combustion vehicles. [10] In the first subchapter, the basic physical relations essential to TEG operation and its construction is explained, then the mathematical model is described.

2.1 Thermoelectric effect

2.1.1 Thermoelectric mechanisms

The operation of TEG is based on three thermoelectric effects: Seebeck effect, Peltier effect, and Thomson effect and it is influenced by Joule heating.

Seebeck effect occurs when the temperature difference is applied to two connected dissimilar thermoelectric materials converting ΔT into electric current. As it is presented on a figure2.1. when both endings of material P and material N are connected with each other and the different temperature is applied to connection points then potential variation will appear. This happens because various materials respond individually to temperature differences. The Seebeck potential difference is defined as[17]:

$$V = \alpha \Delta T \tag{2.1}$$

$$\Delta T = T_{\mathrm{h}} - T_{\mathrm{c}} \tag{2.2}$$

where:

- T_{h} - is the hot side temperature [K],
- T_{c} - is the cold side temperature [K],

- α - is the Seebeck coefficient(material thermopower) [V/K].

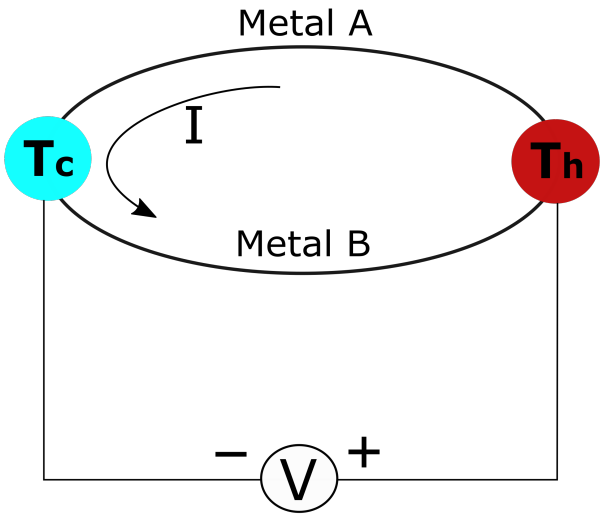

Figure 2.1: Schematic of Seebeck effect in thermocouple.[17]

Peltier effect appears when there is a junction and current is flowing between two different connectors then heat generation occurs (positive or negative depending on the current direction). In order to keep the junction temperature constant, the heat must be added or subtracted. This heat is proportional to the current flow and per unit time it is defined as[17]:

$$\dot{Q} = (\Pi_{\mathrm{A}} - \Pi_{\mathrm{B}})I, \tag{2.3}$$

where:

- I - is the electric current from A to B [A],
- Π_{A} - Peltier coefficient of conductor A [J/C],
- Π_{B} - Peltier coefficient of conductor B [J/C],

It is worthy of mention that total heat generated is not only determined by the Peltier effect but is influenced by the Joule heating.

In semiconductors, the concentration of connection carriers is much stronger temperature-dependent than in metal, therefore in semiconductors, absolute thermoelectric Peltier has definitely higher values than in metals. Therefore, p-n semiconductor types are used in industrial applications.[17]

Thomson effect occurs when across the wire there is a temperature difference and current flows. Then heat is absorbed or released depending on the current direction. Thomson heat is reversible and proportional either to the temperature gradient or the electric current magnitude. The phenomenon characterizes cooling or heating of a current-carrying homogenous material (thereby heat production rate per unit volume) when the temperature gradient is applied according to the following equation[17]:

$$\dot{q} = -\mathcal{K} J \cdot \nabla T \tag{2.4}$$

where:

- ∇T - is the temperature gradient [K/m],
- J - is the current density [A/m^2],
- $\mathcal{K}$ - Thomson coefficient [V/K], which depends on the Seebeck coefficient according the relation:

$$\mathcal{K} = T\frac{d\alpha}{dT} \tag{2.5}$$

Kelvin (Thomson) relationship To get the phenomenon of thermoelectricity it is essential to understand the interrelationships between the abovementioned thermoelectric effect. Based on the first and second laws of thermodynamics, assuming that reversible and irreversible processes are separable, Thomson deduced two relations. The first relation claims that Seebeck, Peltier, and Thomson effects are a different representation of one effect[18]:

$$\mathcal{K} = \frac{d\Pi}{dT} - \alpha. \tag{2.6}$$

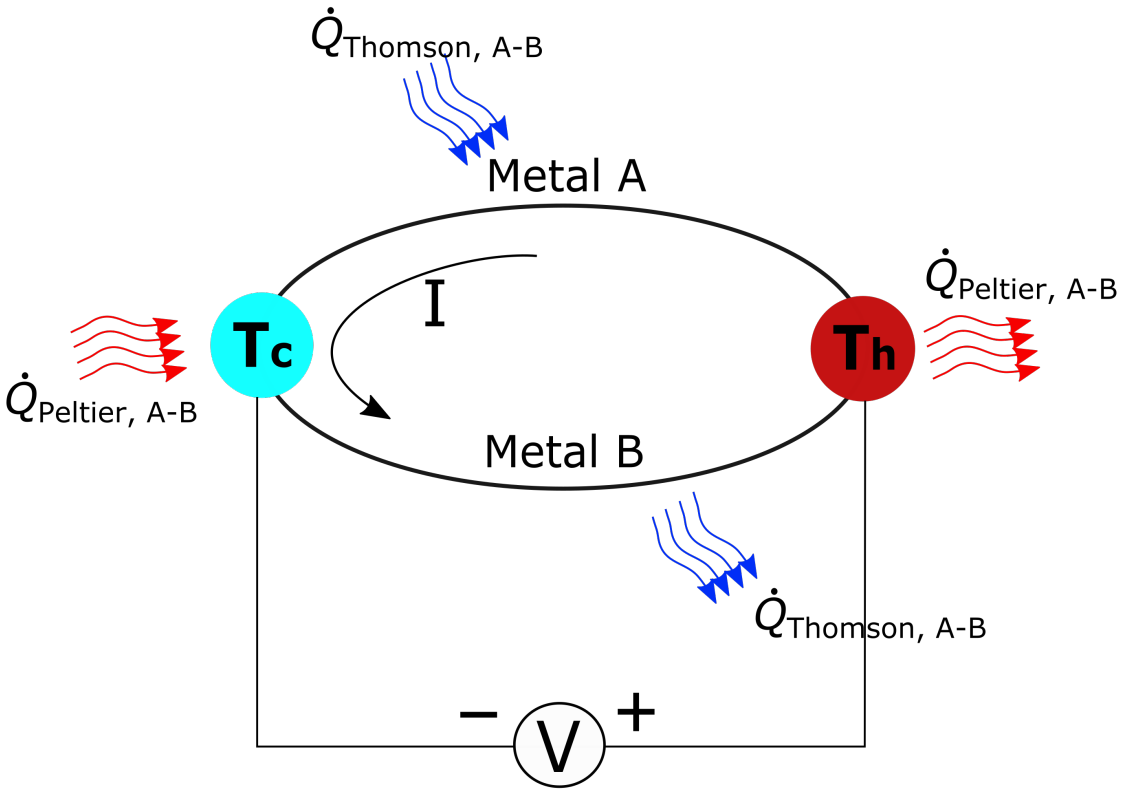

Figure 2.2: Schematic of Peltier and Thomson effects relationship. [17]

The second relation expresses principal connection between Seebeck and Peltier[18]:

$$\Pi = \alpha T \tag{2.7}$$

It is important to mention that for individual material Thomson coefficient can be measured directly, but Seebeck and Peltier coefficients can only be measured for a pair of materials.

Joule heating is the process of heat generation resulted from current flow through the current connector. According to the Joule law the amount of heat generated in the connector when current is flowing is proportional to the product of electrical resistance and square of the current, according to the formula below:

$$Q_{\mathrm{J}} = I^2 R. \tag{2.8}$$

2.1.2 Figure of merit

Heat to power conversion efficiency is measured by a figure of merit ($\mathcal{Z}$) and it is defined as:

$$\mathcal{Z} = \frac{\alpha^2}{\rho k} \tag{2.9}$$

where:

- α - is Seebeck coefficient [V/K],
- ρ - is electrical resistivity [Ohm m],
- k - is thermal conductivity [W/m K], which depends on the Seebeck coefficient according the relation:

As presented in the equation, the figure of merit reflects the relation between the material properties. A high value of the figure of merit provides satisfactory performance for TEG. Low thermal conductivity and electrical resistivity combined with high Seebeck coefficient results in a suitable value of $\mathcal{Z}$. Usually, the performance parameter used for the description of TEG is $\mathcal{Z}T$ which is a multiplication of temperature and figure of merit. $\mathcal{Z}T$ parameter is used for making comparisons between different thermoelectric materials. In figure 2.3 presented below we can observe that the efficiency of thermoelectric is increasing with the increment in value for the figure of merit.

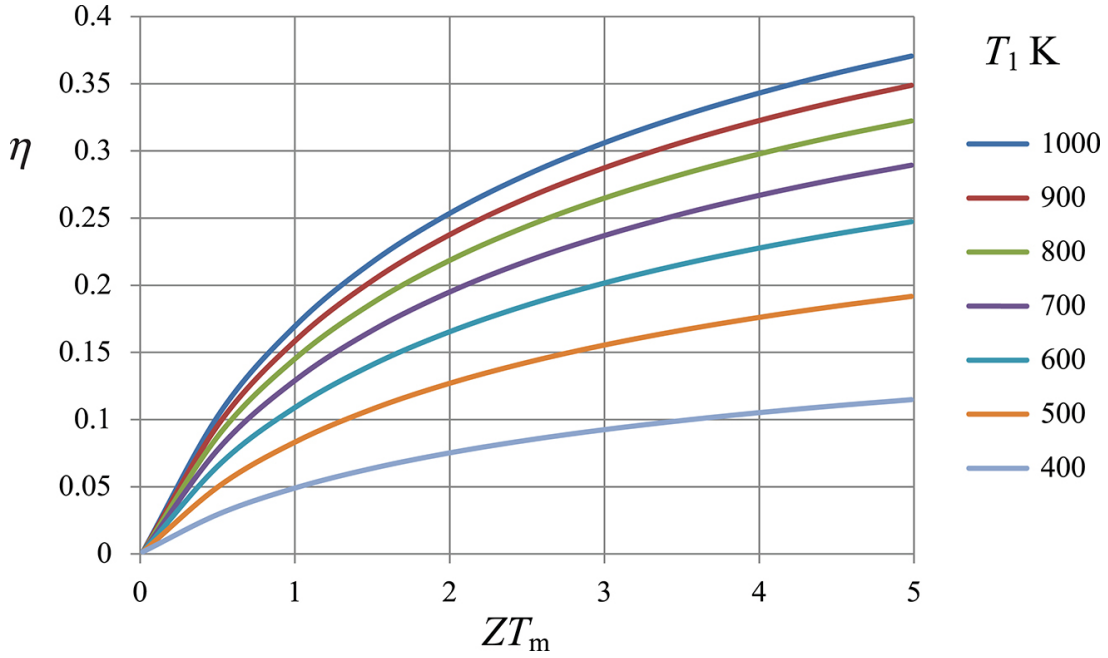

Figure 2.3: Thermoelectric efficiency depending on Figure of Merit and temperature. [19]

2.1.3 Materials

Usually, for both p-type and n-type legs of the thermocouples, the same semiconductor material is used, but not always. In the table 2.1 there are typical semiconductor materials listed, along with the common temperature of its operation and figure of merit value. The most important characteristics of these materials are Seebeck coefficient $\alpha(T)$, resistivity$\rho(T)$, and thermal conductivity $k(T)$, which are strongly temperature-dependent. Sometimes when modeling TEG the averaged values of these three parameters are used but it leads to oversimplification and significant errors.

Table 2.1: The most common semiconductors with figure of merit's properities [17]

Material	Thermocouple type	Temperature ^{o}C	Figure of merit $\mathcal{Z}$ [K^{-1}]
Bi_2Te_3	p	25	2.5 x 10^{-3}
Bi_2Te_3	n	25	2.5 x 10^{-3}
SbBiTeSe	p	70	3.0 x 10^{-3}
BiSbTe	p	150	2.5 x 10^{-3}
Bi_2Te_3-74Sb_2Te_3	n	150	3.0 x 10^{-3}
Bi_2Te_3-25Sb_2Te_3	p	150	2.7 x 10^{-3}
PbTe	n, p	450(325-625)	1.3 x 10^{-3}
ZnSb	p	175	1.4 x 10^{-3}
SiGe	p	1000	0.4 x 10^{-3}
SiGe	n	1000	0.8 x 10^{-3}
GeTe	p	450	1.7 x 10^{-3}
MnTe	p	900	0.4 x 10^{-3}
$CeS_{1.4}$	n	1100	1.8 x 10^{-3}
$AgSbTe_3$	p	400	1.3 x 10^{-3}
InAs	n	700	0.7 x 10^{-3}

2.1.4 TEG

TEGs are consisted of n-type and p-type semiconductor elements, which are connected thermally in parallel electrically in series through copper interconnectors which simultaneously play the role of hot and cold sides of TEG, connecting thermocouples thermally in parallel what can be seen in figure 2.4.[11] Due to the temperature difference between heat and cold side the voltage difference is generated, which forces electrons to flow. In an n-type semiconductor, the electrons flow from hot to the cold side and in p-type semiconductor, the holes move from hot to cold side as presented in the figure below.

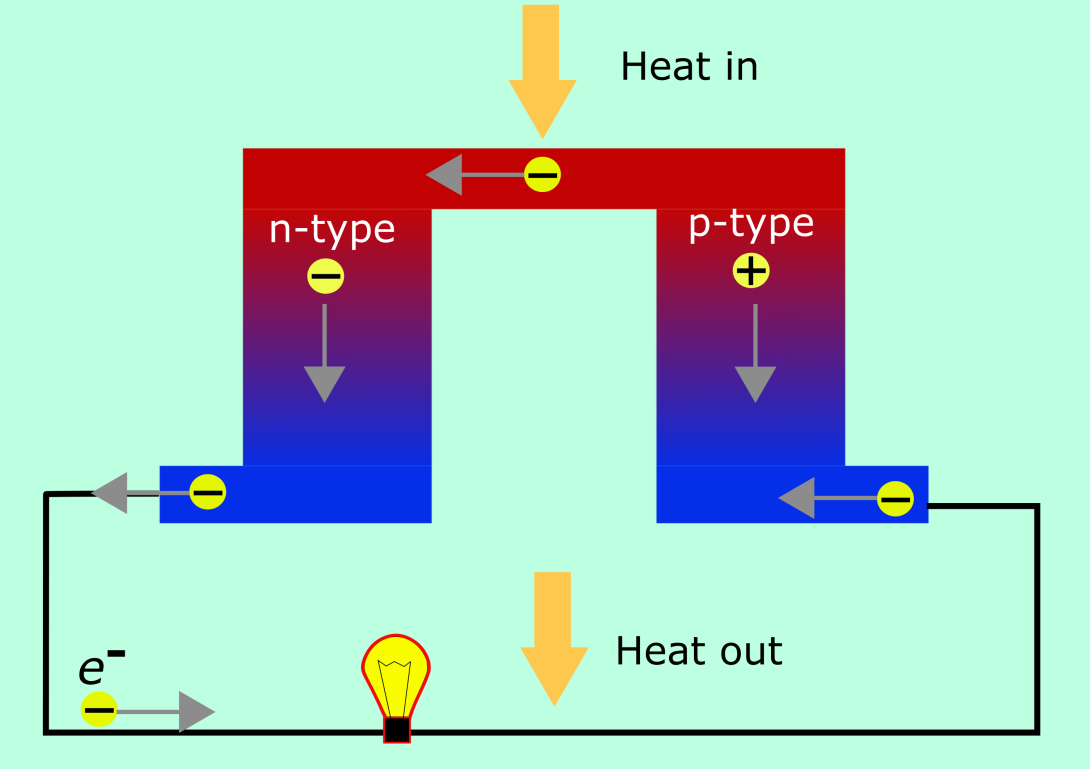

Figure 2.4: Thermoelectric generator operation.

Efficiency

The electrical power generated under the defined load can be calculated according to the following equation, where the R_{Load} is a resistance of any device connected to operating TEG:

$$W = I^2 R_{\mathrm{Load}}. \tag{2.10}$$

The heat flow applied to the hot side is composed of 3 main terms as a result of Seebeck effect, Joule heating, and thermal conduction resulting in the equation:

$$Q_{\mathrm{h}} = \alpha T I - \frac{1}{2} I^2 R + k(T_{\mathrm{h}} - T_{\mathrm{c}}) \tag{2.11}$$

and the thermal efficiency is defined as:

$$\eta = \frac{W}{Q_{\mathrm{h}}} \tag{2.12}$$

which can also be presented in more detailed form based on equations 2.10 and 2.11:

$$\eta = \frac{I^2 R_{\mathrm{Load}}}{\alpha T I - \frac{1}{2} I^2 R + k(T_{\mathrm{h}} - T_{\mathrm{c}})} \tag{2.13}$$

where:

- W - electric power [W]
- I - electrical current load [A],
- R_{Load} - load resistance [Ohm],
- Q_{h} - the heat applied to the system [W], which depends on the Seebeck coefficient according the relation:

The efficiency can also be expressed as the relation between hot and cold side temperatures and figure of merit $\mathcal{Z}$ accordingly:

$$\eta = \frac{\sqrt{1 + \overline{\mathcal{Z}T}} - 1}{\sqrt{1 + \overline{\mathcal{Z}T}} - \frac{T_{\mathrm{c}}}{T_{\mathrm{h}}}} \frac{T_{\mathrm{h}} - T_{\mathrm{c}}}{T_{\mathrm{h}}} \tag{2.14}$$

where $\overline{\mathcal{Z}T}$ is the multiplication of mean figure of merit value and mean legs temperature.

Voltage for TEG is calculated in the following way:

$$V = \alpha(T_{\mathrm{h}} - T_{\mathrm{c}}) = I(R_{\mathrm{Load}} + R) \tag{2.15}$$

Knowing V the current can be easily derived:

$$I = \frac{\alpha(T_{\mathrm{h}} - T_{\mathrm{c}})}{R_{\mathrm{Load}} + R} \tag{2.16}$$

where R is the internal electrical resistivity.

2.2 Mathematical Model

The abovementioned equations and physical characteristics are essential for understanding thermoelectric generator operation. However in order to elaborate an appropriate, well-defined model we need to use more detailed equations than presented in the previous section. Equations, which allow us to describe the charge transport, heat transport and capture a coupled relation between these fields.

2.2.1 Assumptions

The considered numerical simulation concerns a single thermoelement which is the part of the module HZ-14. Within the element, the charge transfer and heat flow are considered. The simulation is steady-state (time-independent) and studied in three dimensions. The physical properties of thermocouples are assumed to be temperature-dependant

2.2.2 Governing equation of thermoelectricity

In order to perform thermoelectric analysis, the coupled equations of continuity of electric charge and heat flow are used as a governing equation:

$$\varrho C \frac{\partial T}{\partial t} + \nabla \cdot q = \dot{q} \tag{2.17}$$

$$\nabla (J + \frac{\partial D}{\partial t}) = 0. \tag{2.18}$$

When coupling the equations 2.17 and 2.18 they form a set of constitutive equations:

$$q = [\Pi] \cdot J - [k] \cdot \nabla T \tag{2.19}$$

$$J = [\sigma] \cdot (E - [\alpha] \cdot T) \tag{2.20}$$

$$D = [\epsilon] \cdot E \tag{2.21}$$

where:

- ϱ - density [kg/m^3]
- C - specific heat capacity [J/(kg K)],
- T - absolute temperature [K],
- $\dot{q}$ - heat generation rate per unit volume [W/m^3],
- q - heat flux vector [W/m^2],

- J - electric current density vector [A/m^2],
- E - electric field intensity vector [V/m^2],
- D - electric flux density vector [C/m^2],
- $[k]$ - thermal conductivity matrix [W/mK],
- $[\sigma]$ - electric conductivity matrix [S/m],
- $[\alpha]$ - Seebeck coefficient matrix [V/K],
- $[\Pi] = T[\sigma]$ - Peltier coefficient matrix [V],
- $[\epsilon]$ - dielectric permitivity matrix [F/m].

For this steady state analysis there is no displacement current ($\frac{\partial D}{\partial t}$), thereby the governing equations looks accordingly:

$$\nabla \cdot q = \dot{q} \tag{2.22}$$

$$\nabla \cdot J = 0. \tag{2.23}$$

The heat flux is an effect of coupling Peltier reversible and Fourrier irreversible effects:

$$q = \Pi J - k\nabla T. \tag{2.24}$$

The generation of current density (J) is affected by Joule effect and Seebeck effect, according to:

$$J = \sigma(E - \alpha\nabla T). \tag{2.25}$$

The electric field is obtained from electric scalar potential:

$$E = -\nabla\phi \tag{2.26}$$

After combining all abovementioned equations the coupled system of equation for thermoelectric steady-state analysis is obtained:

$$\nabla([\Pi] \cdot [J]) - \nabla([k]\nabla T) = \dot{q}, \tag{2.27}$$

$$\nabla \cdot ([\sigma]\nabla\phi) + \nabla \cdot ([\sigma][\alpha]\nabla T) = 0. \tag{2.28}$$

where electrical conductivity σ is defined as $\frac{1}{\rho}$ and Peltier coefficient Π is represented in the form of αT. [20]

After succesful solving process of equations 2.28 and 2.27 we have voltage distribution and temperature distribution which allows us to calculate heat absorbed Q_{h} and volatage difference V. Hence, it is possible to determine the power with the equation 2.10 and conversion efficiency using the equation 2.12.

2.2.3 Boundary Conditions

To solve the differential equation it is essential to set the boundary conditions to specify the determined problem. In this case, there are two differential equations considered in three dimensions. The illustration of thermoelement with boundary conditions is presented in the figures 2.5 and 2.6. The meaning of the symbols used in these graphics is following: cw - ceramic wafer, hs - hot source, cs - cold source, ec - electrical connector, p - p-type leg, n - n-type leg, eg - eggcrate material. Aiming at good grafics visibility the origin of the reference frame was marked with ●.

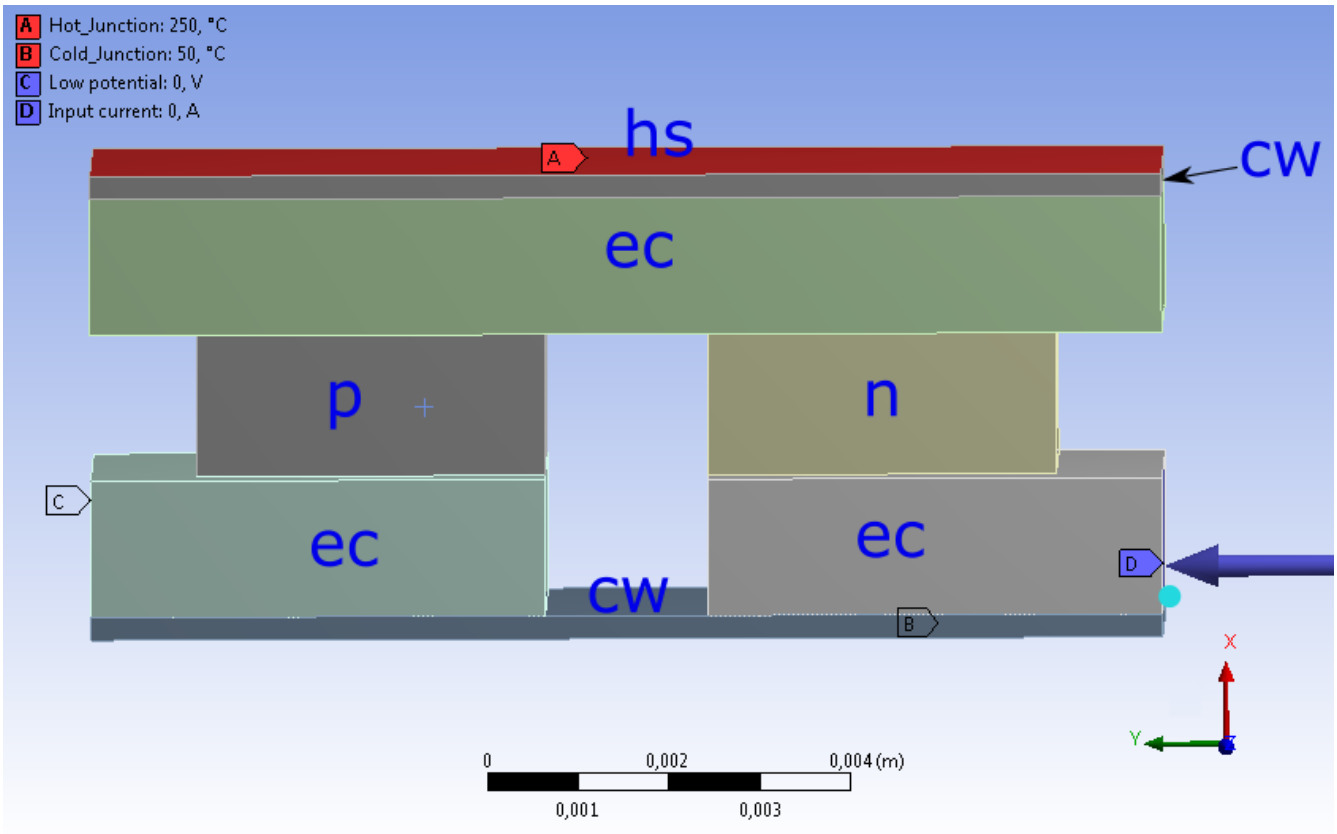

Figure 2.5: Boundary conditions.

The boundary conditions for equation 2.28 are written with the following equations:

$$\begin{aligned} \phi(y = y_{\max})\Big|_{\mathrm{C}} &= 0 \\ J(y = 0)\Big|_{\mathrm{D}} A_{\mathrm{D}} &= I \end{aligned} \tag{2.29}$$

For charge transfer, the voltage on the surface of the copper base at the n-type side (marked with C) is assumed to be zero, and at the p-type side of the copper base outer surface (marked with D) has

a value of current set (which depends on the load condition - arbitrary chosen). The current conductive bodies; p, n, and ec are considered to be one calculation domain for charge transfer, thus on the outer surfaces of the current conductive domain the second type boundary condition is applied:

$$\left.\frac{\partial \phi}{\partial \vec{n}}\right|_{\mathrm{F}} = 0 \tag{2.30}$$

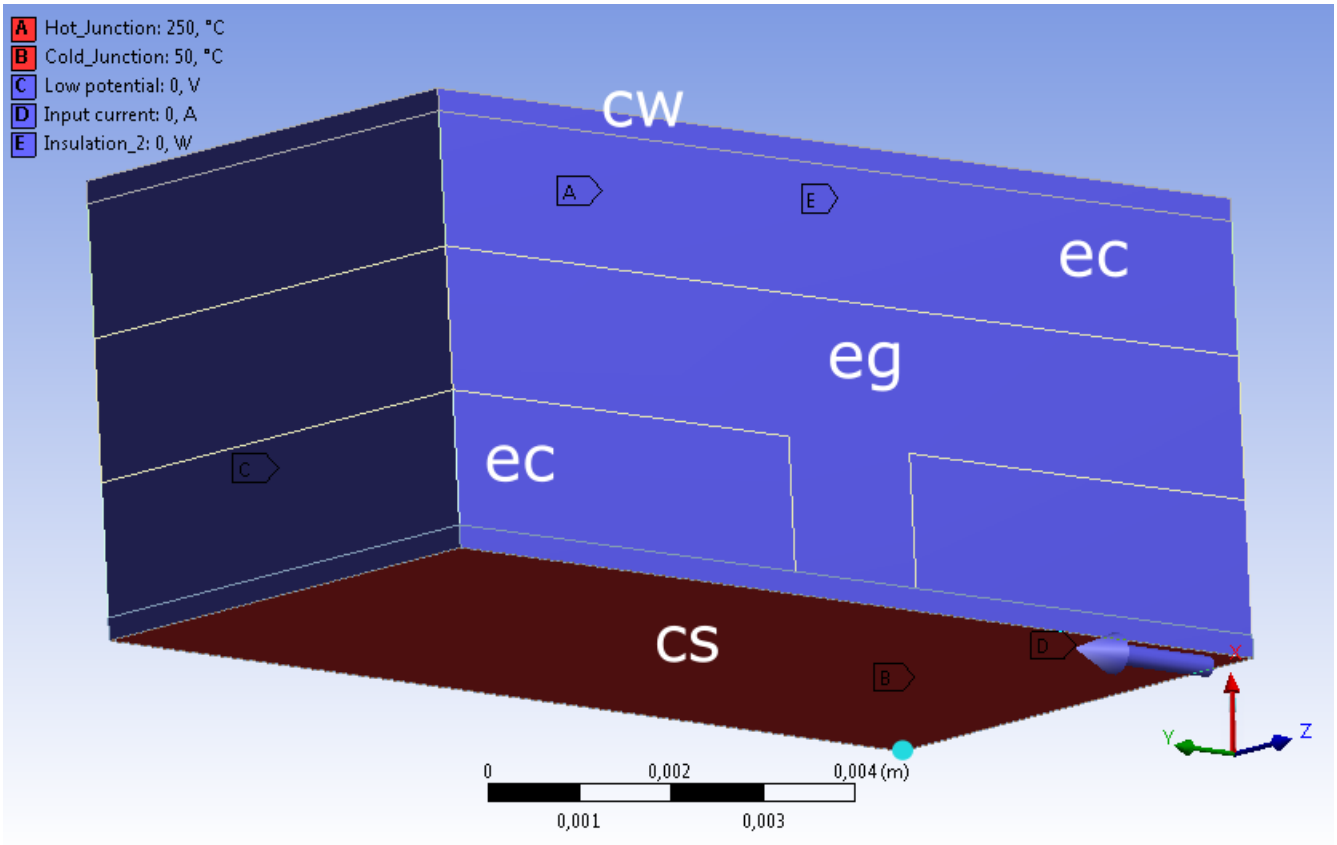

Figure 2.6: Boundary conditions.

For the heat balance equation 2.27; the hot side has a Dirichlet boundary condition on the top and bottom surface (respectively hot and cold side, marked with A and B) as shown on figures 2.5 and 2.6. The values of these boundary conditions are $T_{\mathrm{cold}} = 50^{o}\mathrm{C}$ and $T_{\mathrm{hot}} = 250^{o}rmC$. The other outer surfaces (marked with E) are assumed to be adiabatic, so the second type Neuman boundary condition equal zero is set there as shown in figure 2.6. The heat losses out of one thermoelement are assumed to be negligible because of the structure of the HZ-14 module. As can be seen in figure 2.7 the thermocouples are surrounded by the egg-crate which tightly adheres to thermocouples, so it can be expected that heat losses are scarce.

$$\begin{aligned} T(x = x_{\max})\Big|_{\mathrm{A}} &= T_{\mathrm{hot}} \\ T(x = 0)\Big|_{\mathrm{B}} &= T_{\mathrm{cold}} \\ \left.\frac{\partial T}{\partial \vec{n}}\right|_{\mathrm{E}} &= 0 \end{aligned} \tag{2.31}$$

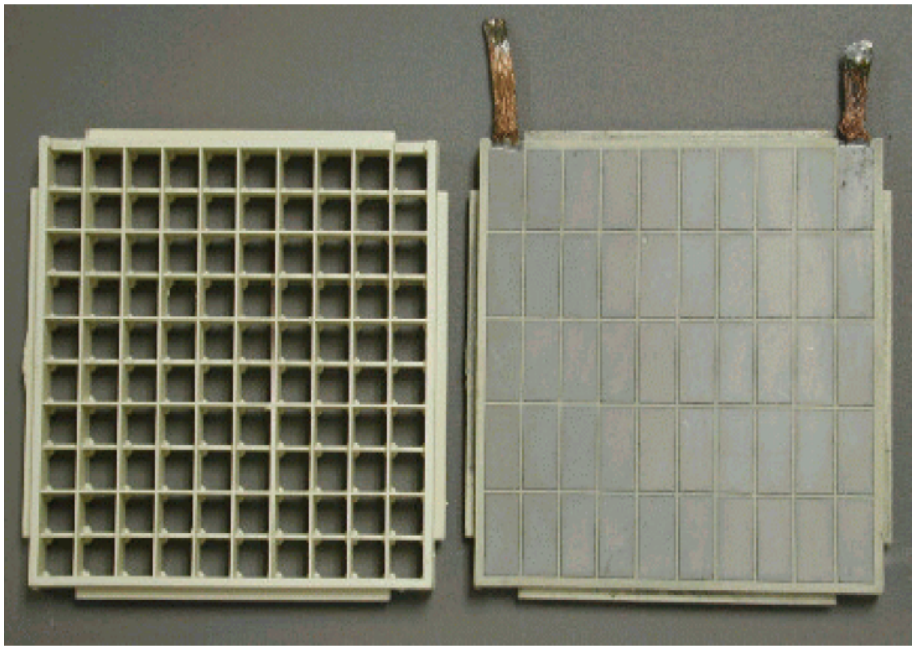

Figure 2.7: Eggcrate construction and HZ-14 module.[21]

2.2.4 Material properties and contact resistances

The performance of the thermoelectric module strongly depends on materials used for its construction. The connectors are always built from copper basically because of its low electric resistivity value, high thermal conductivity value, but also because of its durability, accessibility, and low price. More consideration is needed when choosing the legs (thermocouples) material. As it was shown in the table 2.1 various semiconductors have different performance and operating temperature window. That is why, when constructing a thermoelectric module it should be taken into account, what operating conditions are expected. In our case, the HZ-14 module[16] was designed to harvest low quality heat, so its upper limit for operating temperature is 350 ^{o}C. The material from which p-type and n-type thermocouples are constructed is Bi_2Te_3. It is important to know that TEGs copper connectors are mostly covered with ceramic wafer composed from alumina (Al_2O_3) to prevent TEG from corrosion.

When modeling thermoelement it is essential to incorporate the temperature-dependent properties for semiconductor materials instead of assuming a constant value. This approach needs a numerical approximation of the thermal dependency of material properties. It makes the numeric code more complicated but improves the quality of results significantly, because $\alpha(T)$, $\rho(T)$ and $k(T)$ vary significantly with temperature [8],[11]. Temperature-dependent physical properties of Bi_2Te_3 can be described by using below-written polynomial:

.

$$A(T) = \sum_{3}^{i=0} a_i T^i \tag{2.32}$$

where the polynomials coefficients take the following values:

The curves shape for the Seebeck coefficient, electric resistivity, and thermal conductivity of Bi_2Te_3 semiconductor material are plotted in the figures 2.8. The properties of copper and alumina are assumed

Table 2.2: Temperature-dependent semiconductor materials properties [8]

Property name	$A(T)$	a_0	a_1	a_2	a_3
Seebeck coefficient (V/K)					
p-type	$\alpha_{\mathrm{p}}(T)$	$-274.4 \cdot 10^{-6}$	$2.422 \cdot 10^{-6}$	$-0.003724 \cdot 10^{-6}$	$0.5921 \cdot 10^{-12}$
n-type	$\alpha_{\mathrm{n}}(T)$	$-8.959 \cdot 10^{-6}$	$0.9272 \cdot 10^{-6}$	$-0.001075 \cdot 10^{-6}$	$-0.1292 \cdot 10^{-12}$
electric resistivity ($\Omega\mathrm{m}$)					
p-type	$\rho_{\mathrm{p}}(T)$	$-2.245 \cdot 10^{-5}$	$1.388 \cdot 10^{-7}$	$-1.251 \cdot 10^{-10}$	$0.2249 \cdot 10^{-13}$
n-type	$\rho_{\mathrm{n}}(T)$	$-1.05 \cdot 10^{-5}$	$0.9103 \cdot 10^{-7}$	$-0.6429 \cdot 10^{-10}$	$-0.1249 \cdot 10^{-13}$
thermal conductivity (W/mK)					
p-type	$k_{\mathrm{p}}(T)$	-2.363	0.03874	$-12.43 \cdot 10^{-5}$	$12.52 \cdot 10^{-8}$
n-type	$k_{\mathrm{n}}(T)$	3.237	-0.01243	$2.124 \cdot 10^{-5}$	$-0.9998 \cdot 10^{-8}$

to be temperature independent as well as the egg-crate material can be found in the table 2.3.

Table 2.3: Materials properties [16]

Element type	Material	electric resistivity ($\Omega\mathrm{m}$)	thermal conductivity (W/mK)
current conector	Cu	$2,63 \cdot 10^{-8}$	285
ceramic waffer	Al_2O_3	-	23
eggcrate material	Hi-Tech custom material	-	$0,1$

The knowledge about material properties is essential because it enables us to estimate the thermal and electrical resistances in our thermoelement. These resistances are the main factor which influences TEGs performance. The scheme of electrical and thermal resistances is presented in figures 2.9 and 2.10.

Contact Resistances

Heat transfer and electrical conduction across the TEG are accompanied byr electric and thermal losses. As it is known from basic physics the higher electric resistance and the lower thermal conductivity, the worst is the performance of our device. Unfortunately, material resistance losses are not the only ones that affect thermoelement performance. One of the important factors when modeling TEG is to consider contact resistance between adjacent elements. This type of loss can significantly decrease TEG performance. In the figure 2.9 the contact electrical resistances are also included (R_l).

In literature [22] and [11] it is reported that no contact resistance should be neglected when modeling thermoelements, however, the values of contact resistances available in the literature vary between each other. For this analysis, the corresponding value of contact resistance between the copper current connector and semiconductor legs is assumed to be $4.8 \times 10^{-9}\ \Omega\mathrm{m}^2$.[22]

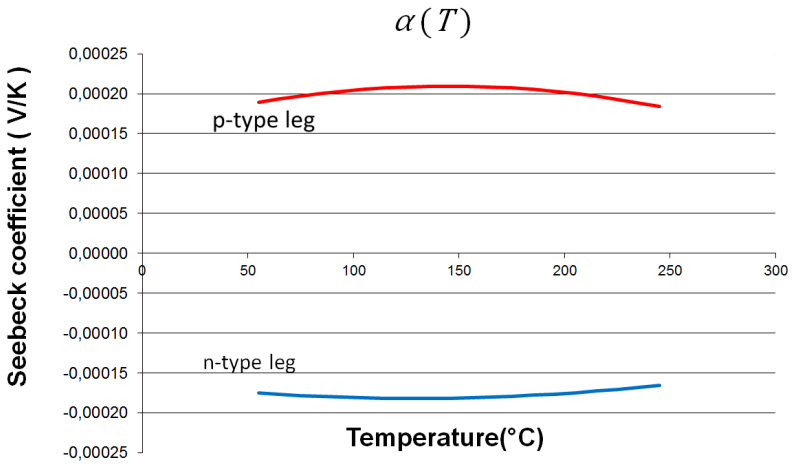

(a) Bi_2Te_3 Seebeck coefficient

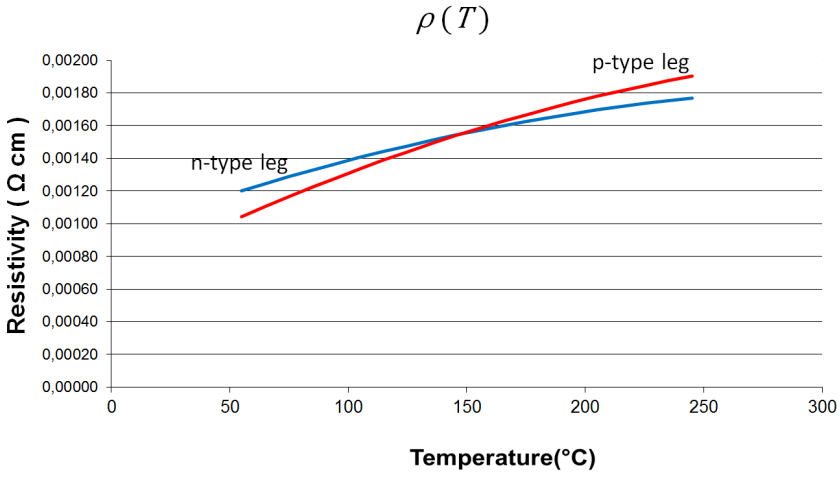

(b) Bi_2Te_3 Resistivity

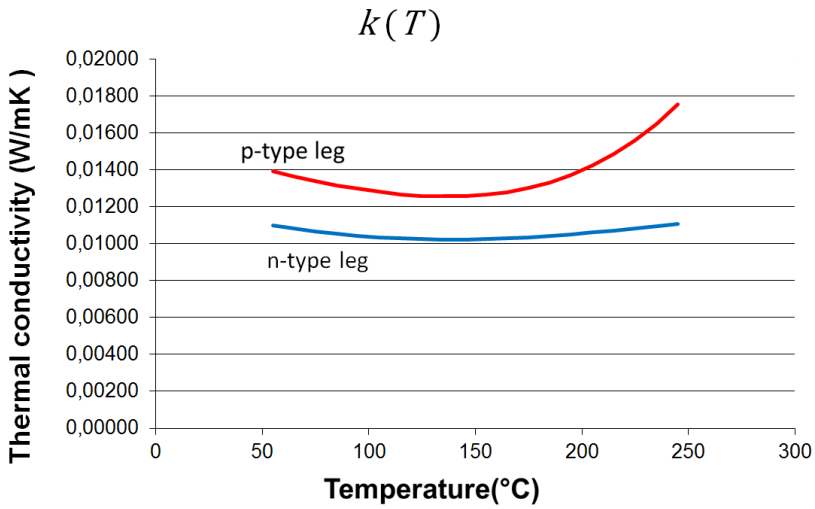

(c) Bi_2Te_3 Thermal conductivity

Figure 2.8: Bi_2Te_3 material properities

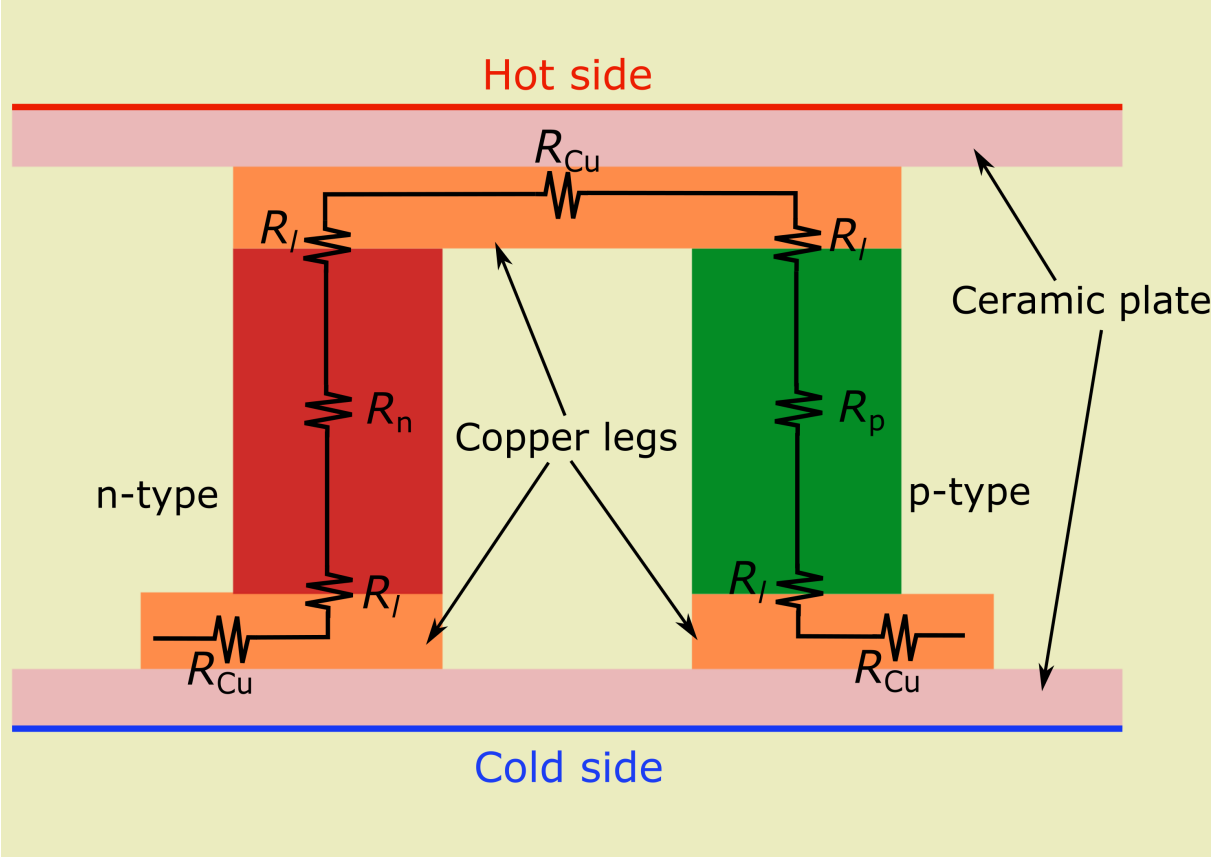

Figure 2.9: TEG - electrical resistances

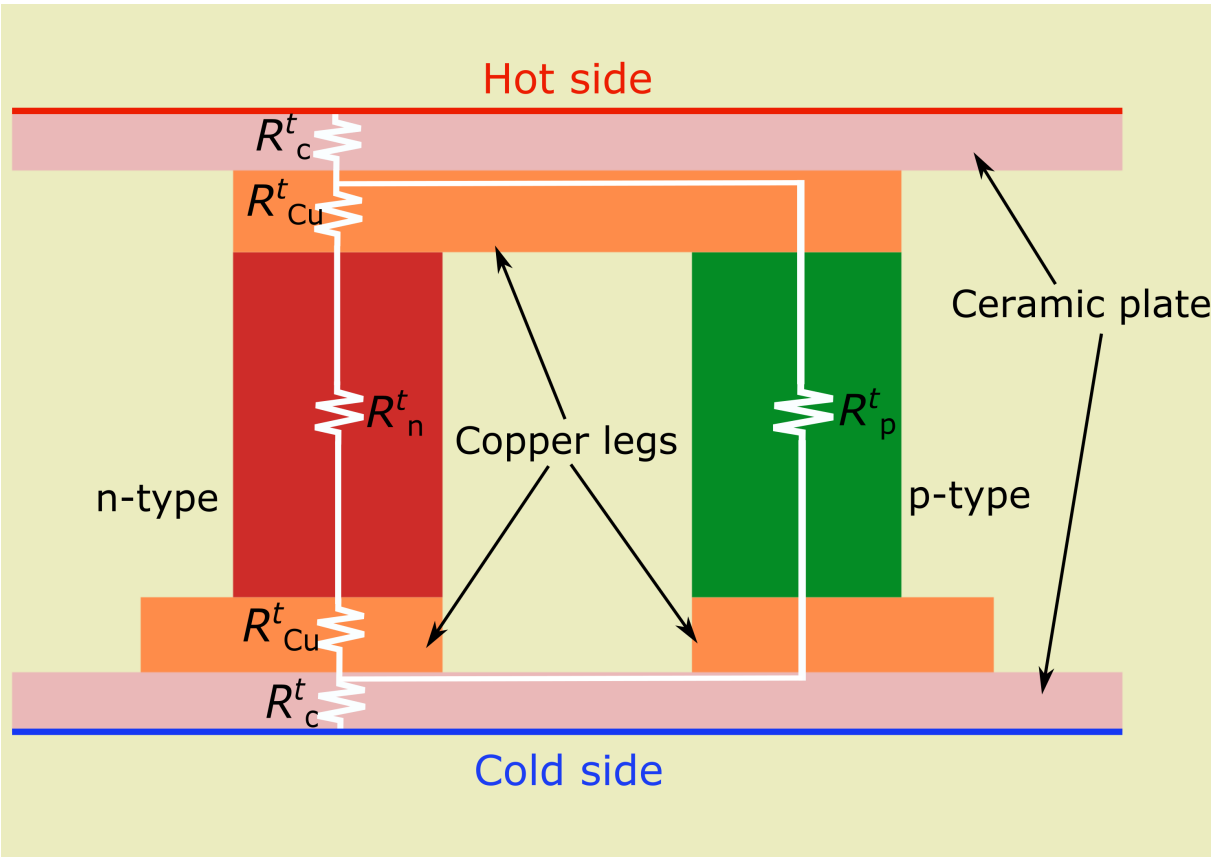

Figure 2.10: TEG - thermal resistances

Chapter 3

Numerical Implementation

In the study, the HZ-14 commercial module was simulated. To simplify the problem, only the one thermoelement is simulated instead of the whole module. The geometry was prepared using Design Modeler software based on data derived from [16]. For the numerical implementation process, ANSYS Workbench was used. The mesh was prepared with the Mesh module in ANSYS. Then the obtained data were analyzed and plotted using Matlab and Microsoft Excel software.

3.1 Thermoelement geometry

There were two versions of geometry prepared. The first one including only single thermoelement, composed from the top and bottom copper bases and n-type and p-type semiconductors, as shown in the figure 3.1(a). The second version consisted of single thermoelement described before, ceramic wafers, and part of the egg-crate surrounding legs 3.1(b). The second version was created as it was cut out from the module. For the simulation the second version was used in order to faithfully reproduce the real device.

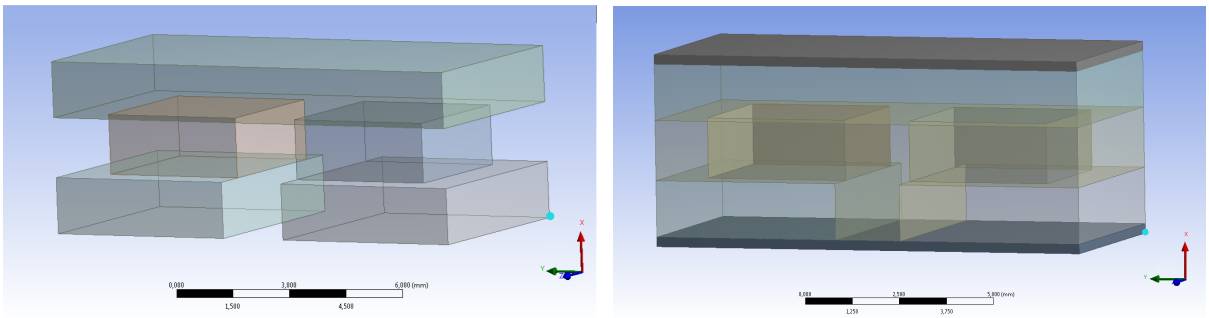

(a) 1st geometry.

(b) 2nd geometry.

Figure 3.1: Models geometry.

The dimensions of the elements are shown in the figures 3.2 and 3.3. The unit is milimeters.

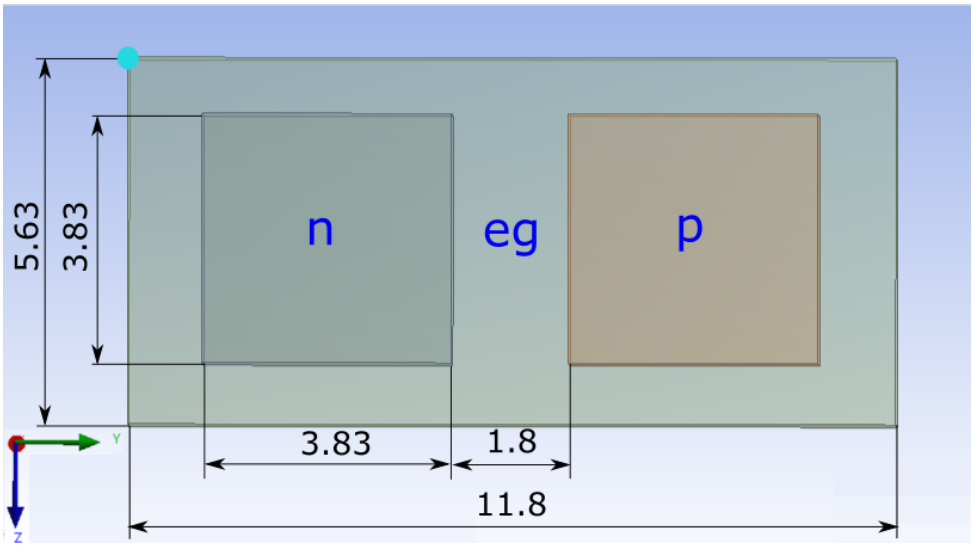

Figure 3.2: The thermocouple dimensions I.

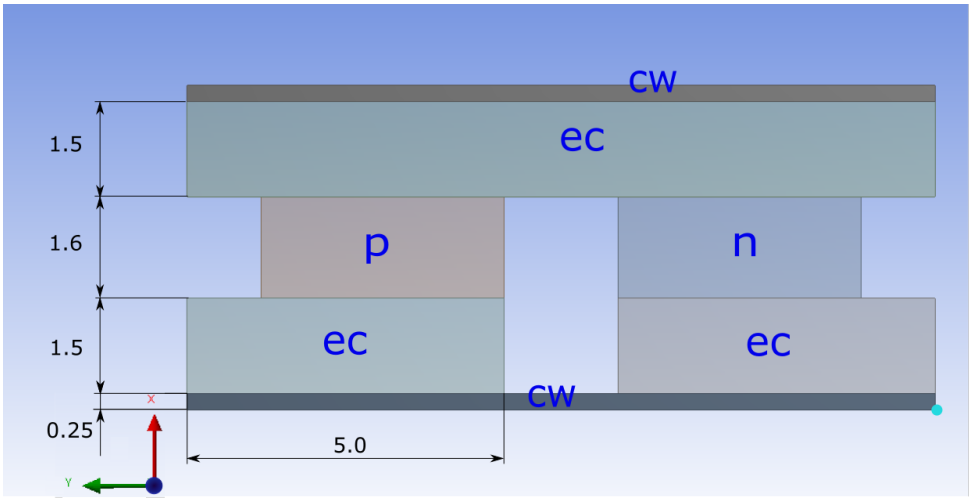

Figure 3.3: The thermocouple dimensions II.

3.2 Meshing - elements definition

The presented geometry is the calculation domain in which the charge and temperature fields will be calculated. To apply numerical equations, there is a need to define elements. The defined geometry was divided into 6020 cuboid elements what gave 30 000 nodes, as presented in figure 3.4. The elements size is 0,38 x 0,375 x 0,27 mm. The mesh could not be refined into smaller elements because the ANSYS student license has the limit of 32 000 nodes for finite element method.

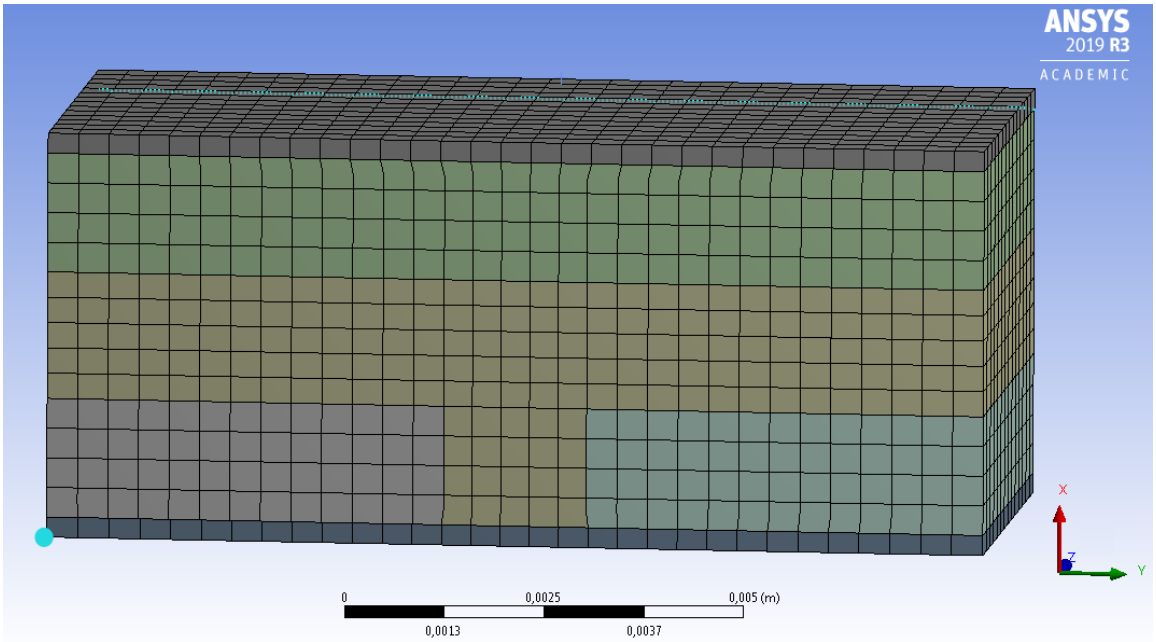

Figure 3.4: The mesh for thermoelement and eggrcrate.

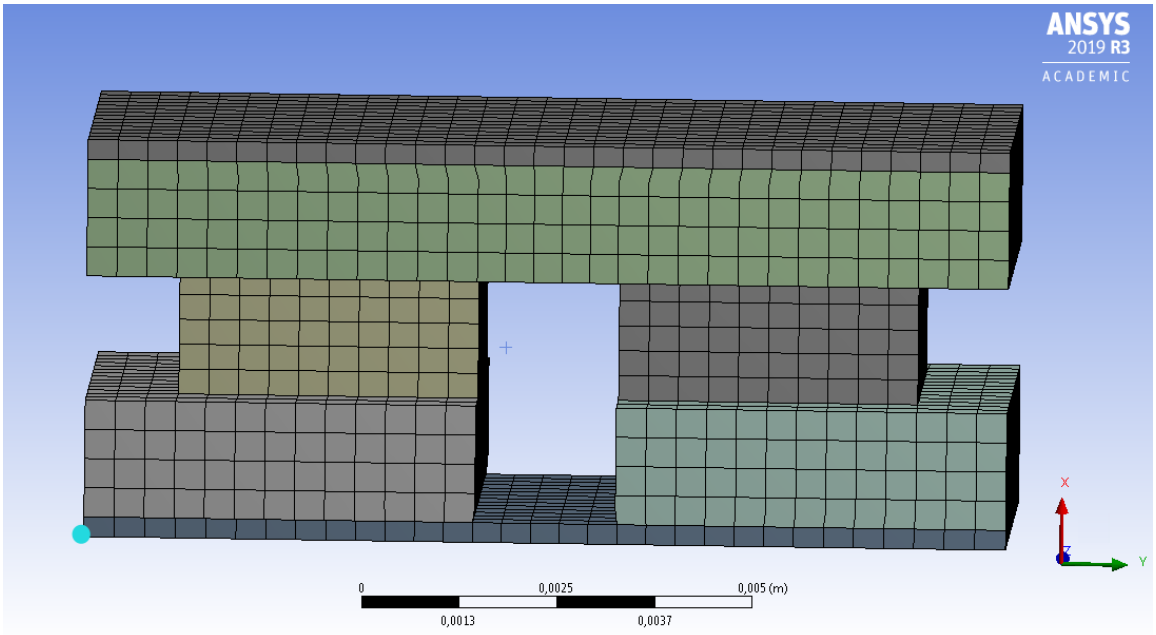

Figure 3.5: The mesh for thermoelement.

3.3 Numerical Model

In order to solve the equations 2.28 and 2.27 in the calculation domain, the most common way is to implement numerical procedure and code it. Fortunatelly there are many commercial softwares which enable us to use their Graphical User Interface without the need to elaborate code literally. One of the most popular software is ANSYS Workbench, which was used to prepare the model for this thesis. The Finite Element Method has become a standard technique in solving engineering problems. The method can model complicated shaped structures, composed from complex materials and impose different types

of boundary conditons. FEM is easily adaptable to various sets of constitutive equations, what makes it very convenient tool for coupled physics simulation. For the described mathematical model the thermal-electric coupled physics library was used.

3.3.1 Numerical scheme

To solve two coupled governing equations with finite element method, equations 2.27 and 2.28 should be firstly transformed according to the Galerkin FEM techniques. This procedure is based on approximation of physical unknowns (T and ϕ) over a single finite element.[20]

$$T = N \cdot T_e \tag{3.1}$$

$$\phi = N \cdot \phi_e \tag{3.2}$$

where:

- T_e - vector of nodal temperatures,
- ϕ_e - vector of nodal electric potentials,
- N - vector of element shapes functions.

After the application of Galerkin weighting scheme[23], the differential equations 2.27 and 2.28 are transformed into algebraic equation given below (assuming steady-state conditions):

$$\begin{bmatrix} K^{TT} & 0 \\ K^{\phi T} & K^{\phi\phi} \end{bmatrix} \begin{Bmatrix} T_e \\ \phi_e \end{Bmatrix} \begin{Bmatrix} Q + Q^P + Q^e \\ I \end{Bmatrix} \tag{3.3}$$

where:

- $K^{TT} = \int_V \nabla N \cdot [k] \cdot \nabla N dV$ - thermal stiffness matrix,
- $K^{\phi T} = \int_V \nabla N \cdot [\sigma] \cdot [\alpha] \cdot \nabla N dV$ - Seebeck stiffness matrix,
- $K^{\phi\phi} = \int_V \nabla N \cdot [\sigma] \cdot \nabla N dV$ - electric stiffness matrix,
- $Q^P = \int_V \nabla N \cdot [\Pi] \cdot \nabla N dV$ - vector of Peltier heat load,
- $Q^e = \int_V NE \cdot J dV$ - vector of electric power load,
- Q - vector of combined heat generation loads,
- I - vector of electric current load.

It is important to know that the Joule heat vector (Q^e) is obtained from the electrical fragment of the solution. In the case of the electrical part, the stiffness matrix ($K^{\phi\phi}$) contains the material electrical properties which are temperature dependent, thereby it uses the thermal part of the solution. That is how the charge equation and temperature equation are coupled.[24] The system of formed equations is solved with ANSYS Mechanical iterative solver.

3.3.2 Boundary conditions

Vector of thermal heat generation loads (Q) arises from the boundary condition, and can be imposed as a heat flow rate at the boundary or as a fixed temperature. In our case the fixed temperature was chosen. Similarly, the electric current load (I) which can be set either by electric potential or electric current. [20]

3.3.3 Material properties

The input matrices with the material properties are in the form of diagonal elements of the coefficients along the x, y, z, axes. In our case the material properties are temperature-dependent but the materials are isotropic so the properties are the same in each direction for a given temperature. The electrical conductivity [σ] is obtained internally via conversion of electrical resistivity [ρ]. It is worthy of mention that although the Thomson effect is not visible in the before-mentioned equations however, it is taken into account internally through the definition of temperature-dependent Seebeck coefficient [α]. The contact resistances were included with the help of an in-build tool for contact modeling in ANSYS thermal-electric.

3.3.4 Module performance

As it was presented before, the analyzed HZ-14 module consists of 49 thermoelements. Although, for the simplicity of the analysis, only one thermocouple was simulated. It should be taken into consideration that ANSYS Workbench academic version has element number limits. Bearing in mind that thermocoples are connected electrically in series and thermally in pararel, the performance of the complete TEG was derived from the simulation output of a single thermoelement. Thus, the voltage drop induced by a given current in single element was multiplied by its number (49). That is how, the voltage drop for the module was obtained.

Chapter 4

Results and discussion

The process of model development was conducted iteratively. In the beginning, two basic models were prepared. Based on conclusions from two first versions of the model the final 3rd version was developed. All the versions are 3-dimensional models, having the same geometry and boundary conditions as presented in chapter 3.

In the first one, the physical properties were averaged to obtain constant non-temperature-dependent values and compared with the experimental data provided by $Hi - Z\ Technology$ - the HZ-14 thermoelectric module manufacturer. Since the results were not tolerable, the second model included nonlinear temperature-dependent material properties, which also has not given adequate results. Then after the literature survey, the full model was elaborated. Apart from nonlinear material properties, the final model has implemented contact resistance described in the 2.2, which led to the satisfactory performance of the analysis. In this chapter, the model's output is described along with a detailed analysis of the final model.

4.1 Basic models

1st model The physical properties of legs material and connectors were obtained by averaging the data available in [25] and presented in figure 2.8. To check the model performance the results of the numerical analysis were presented in the form of power and efficiency curves in the function of current (I) and compared with corresponding curves from the experiment, which is presented in the figure below.

As can be seen, the model considerably overestimates the power produced by the module and thus the efficiency as well. When operating, in legs of TEG the huge temperature gradient appears so in almost every point of the legs the temperature is different so it can be the wrong approach to use the averaged materials properties. Moreover, the omission of voltage loss generated onto contact resistance plays also a significant role in the results.

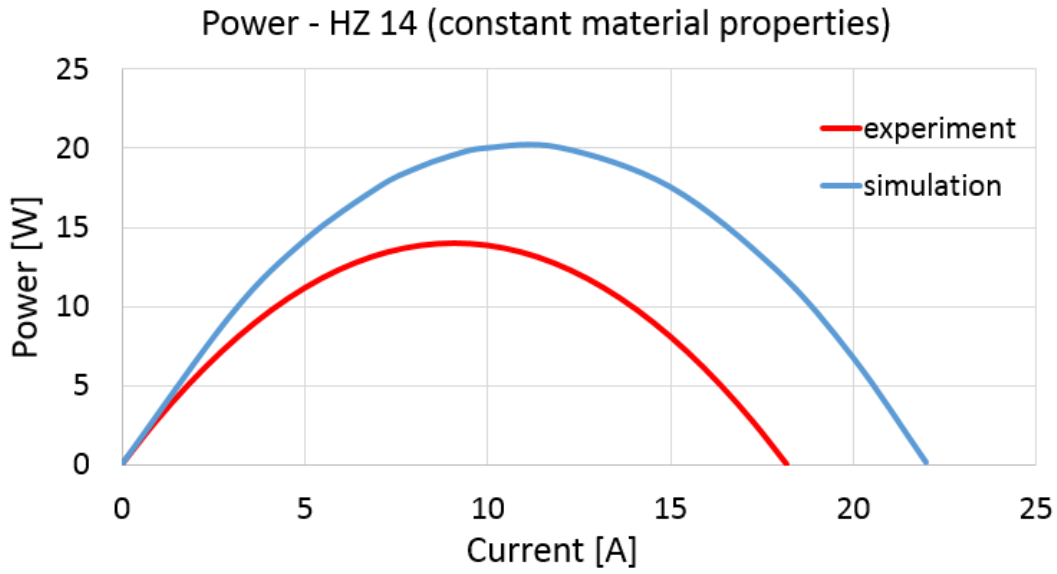

Figure 4.1: First HZ 14 model, power curve performance compared with experiment.

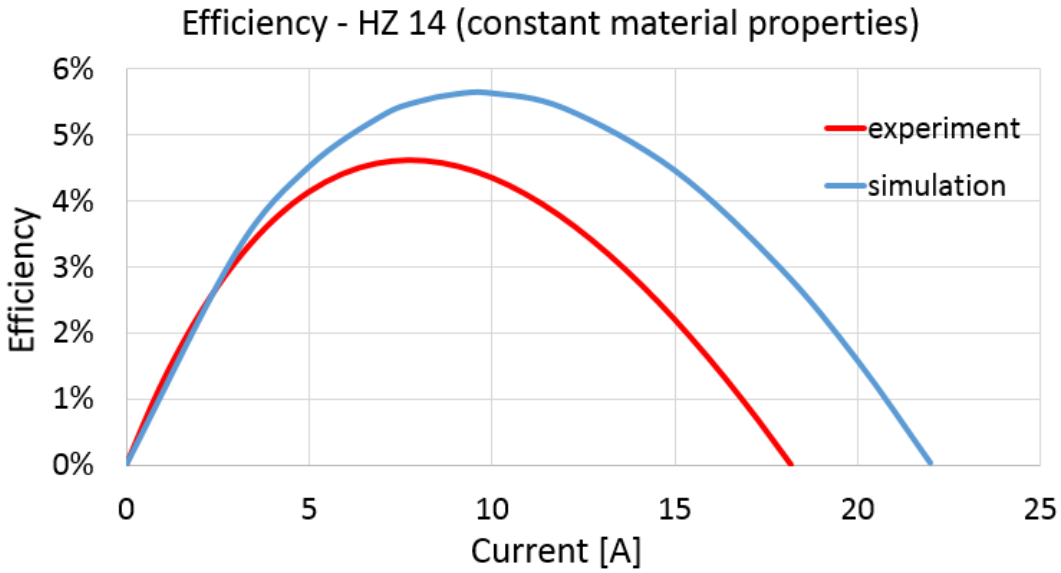

Figure 4.2: First HZ 14 model, efficiency curve performance compared with experiment.

2nd model The second model is almost the same as the first one with one difference that physical properties of the materials are assumed to be nonlinear and temperature dependent according to data presented in the tables 2.2 and 2.3. The comparison of model output with experiment is presented below.

The performance of the 2nd model as in the first case predicts much higher values of power and efficiency than in real device. Thus it can be deduced that the implementation of nonlinear material properties does not improve the results significantly.

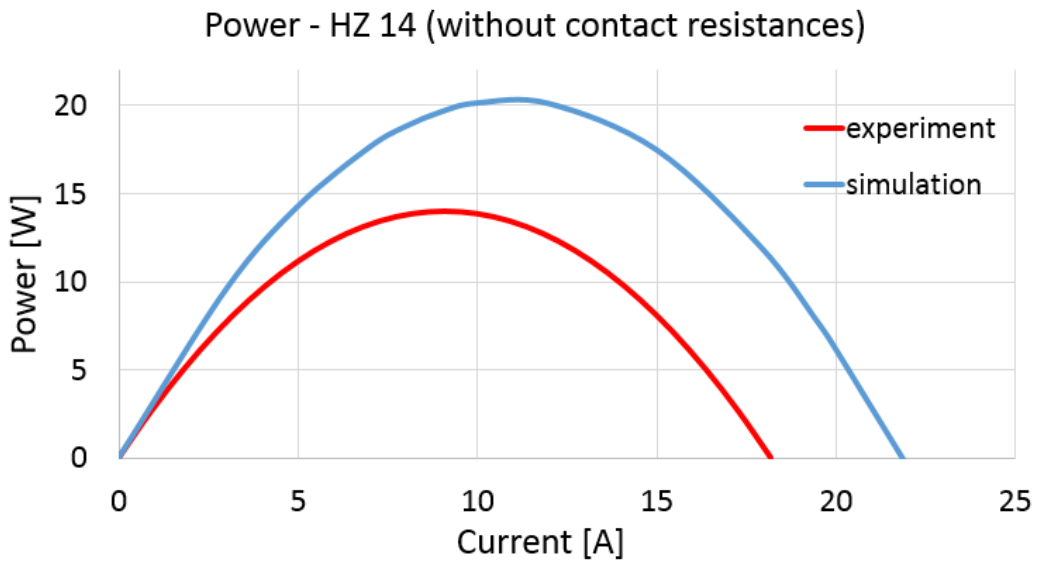

Figure 4.3: Second HZ 14 model, power curve performance compared with experiment.

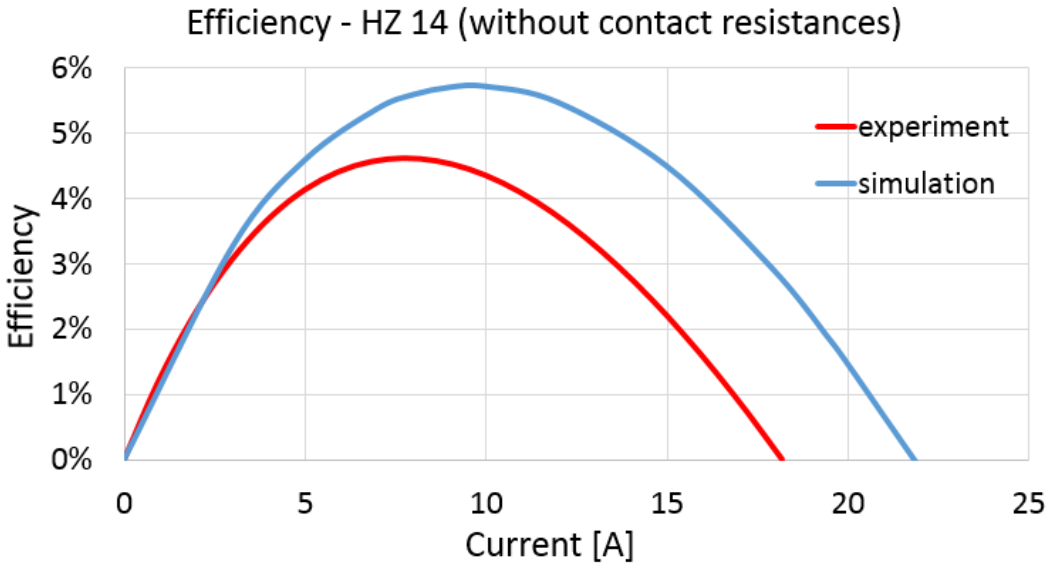

Figure 4.4: Second HZ 14 model, efficiency curve performance compared with experiment.

4.2 Full model - performance

3rd model The final version of the numerical model prepared in ANSYS Workbench consist of a mathematical description of heat and charge transfer in a single thermocouple. The material properties, like the Seebeck coefficient, electric resistivity, and thermal conductivity are described by non-linear, temperature dependent functions. The contact resistances between thermocouple legs and electric connectors are included. As it can be seen in the figures 4.5 and 4.6, the final version of the model predicts the shape of power and efficiency curves with a satisfactory margin. Thus, the model can be used for some parametric studies. In the figure 4.7 the electrical load resistance is presented. From the graphics it can be seen that simulated power response under the applied resistance is higher than in the real device.

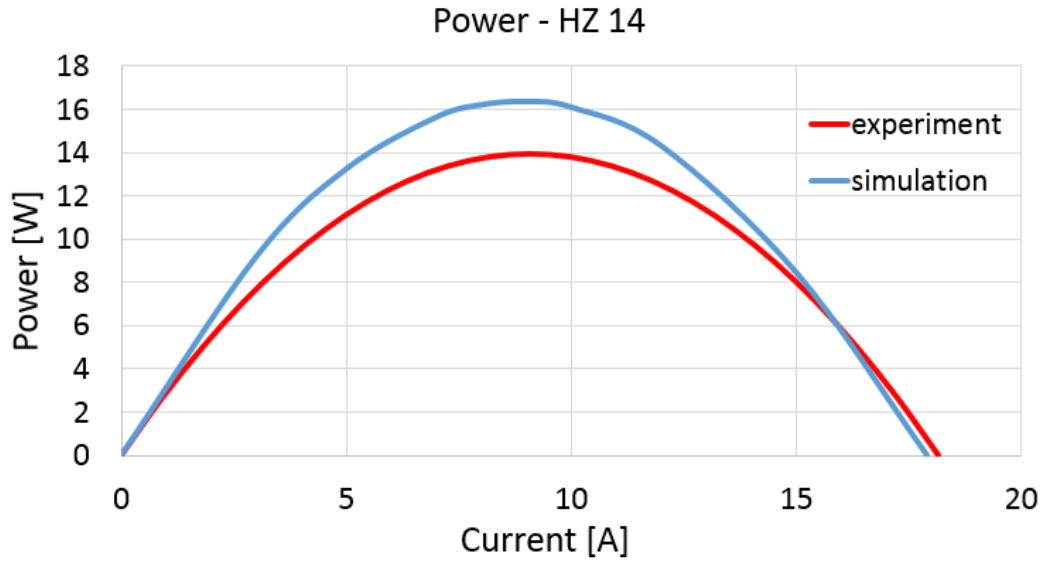

Figure 4.5: Full HZ 14 model, power curve performance compared with experiment.

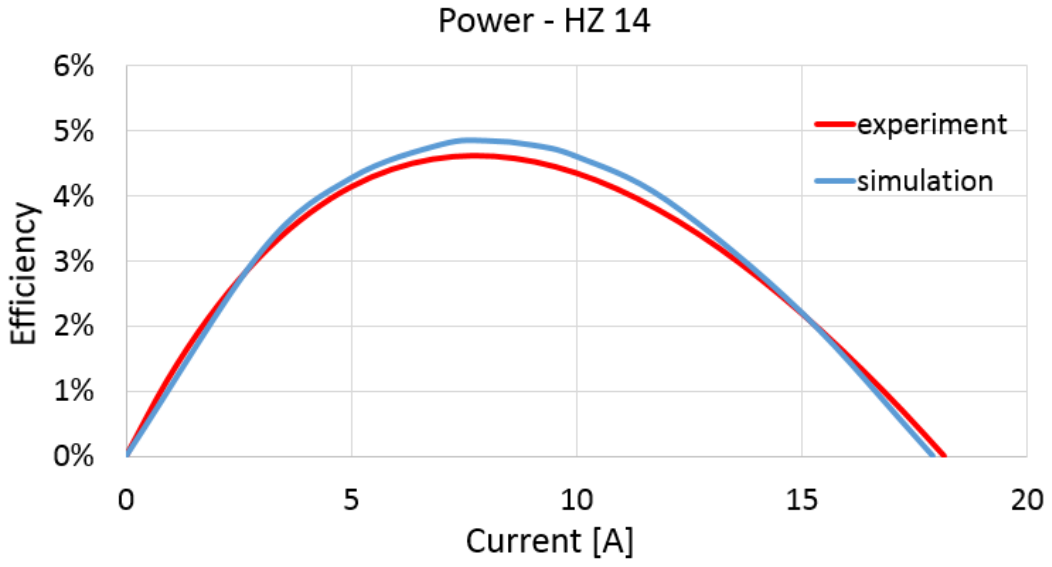

Figure 4.6: Full HZ 14 model, efficiency curve performance compared with experiment.

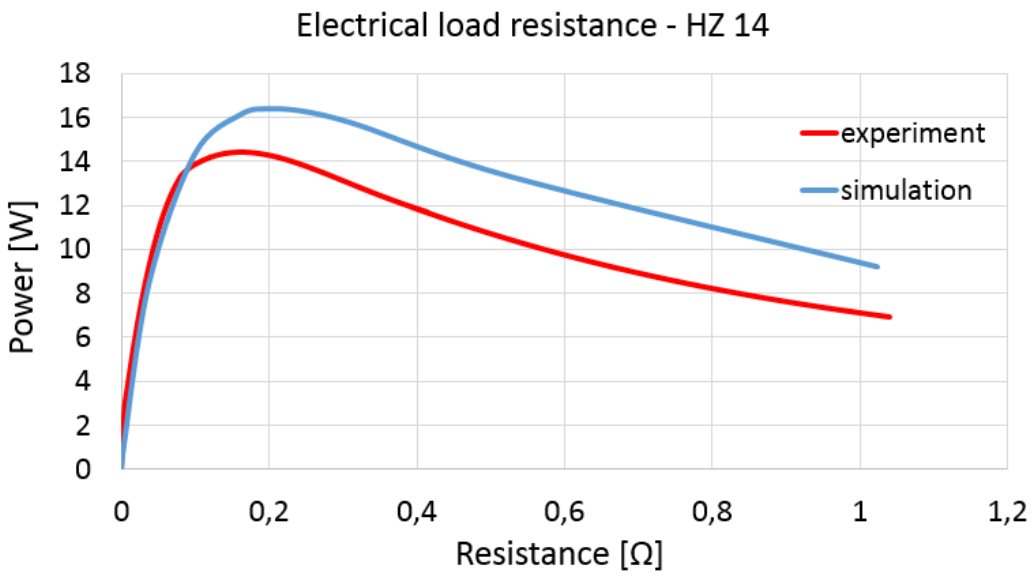

Figure 4.7: Full HZ 14 model, load resistance curve performance compared with experiment.

4.3 Models comparison

In the figures below all three approaches are presented with each other. The power curves 4.8 and efficiency curve 4.9 for all the three models are presented with each other. On the figures, we can see that although the inclusion of nonlinear material characteristics does not change the model output much, the incorporation of contact resistance between legs and copper connectors influences the output significantly.

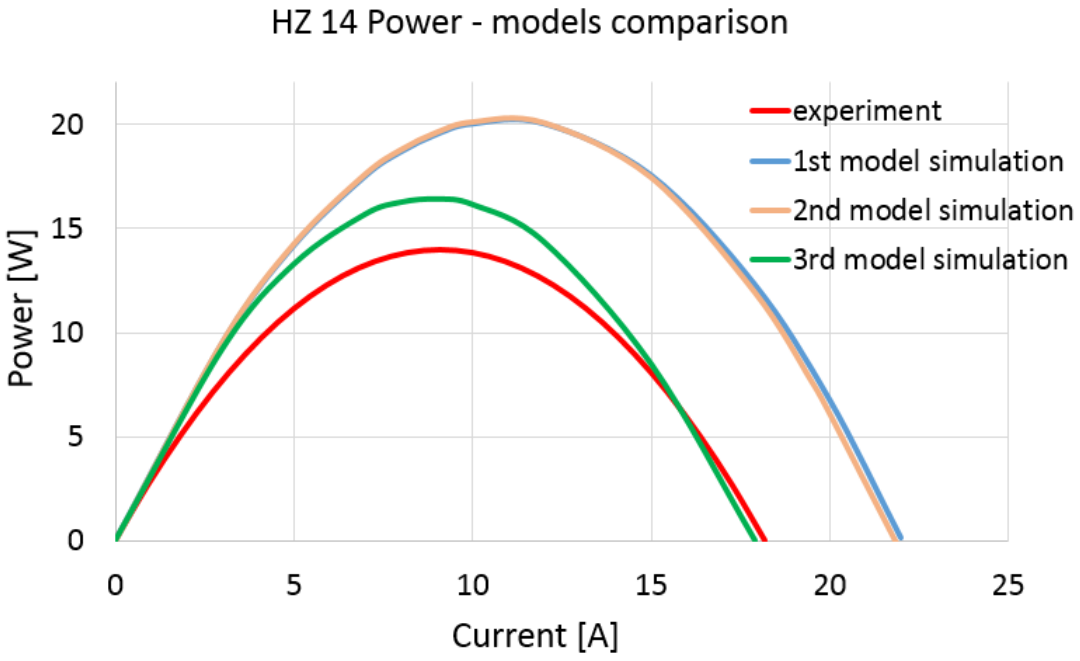

Figure 4.8: Models comparison, power curve performance compared with experiment.

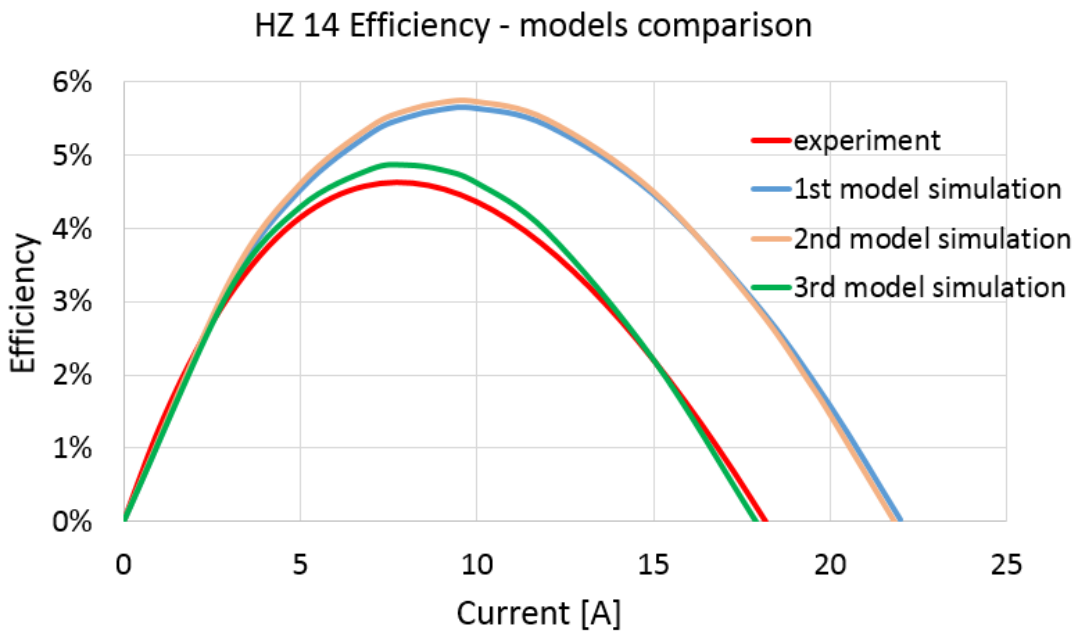

Figure 4.9: Models comparison, efficiency curve performance compared with experiment.

The results for the module power are quite higher than the experiment output. This may be the result of the chosen methodology. As was mentioned before the simulation was performed for only one thermocouple and then the voltage difference was multiplied by the number of thermocouples. This approach could not take into account a few more phenomena occurring in the module. These could be for example slightly different temperature distribution at thermocouples placed in different locations within the module or the additional ohmic losses on interconnectors. Moreover, The data used in the presented approach (values of contact resistance) could not be precise enough to perform an accurate simulation. The efficiency curve 4.9 follows similar rules as the power curves because they relate with each other.

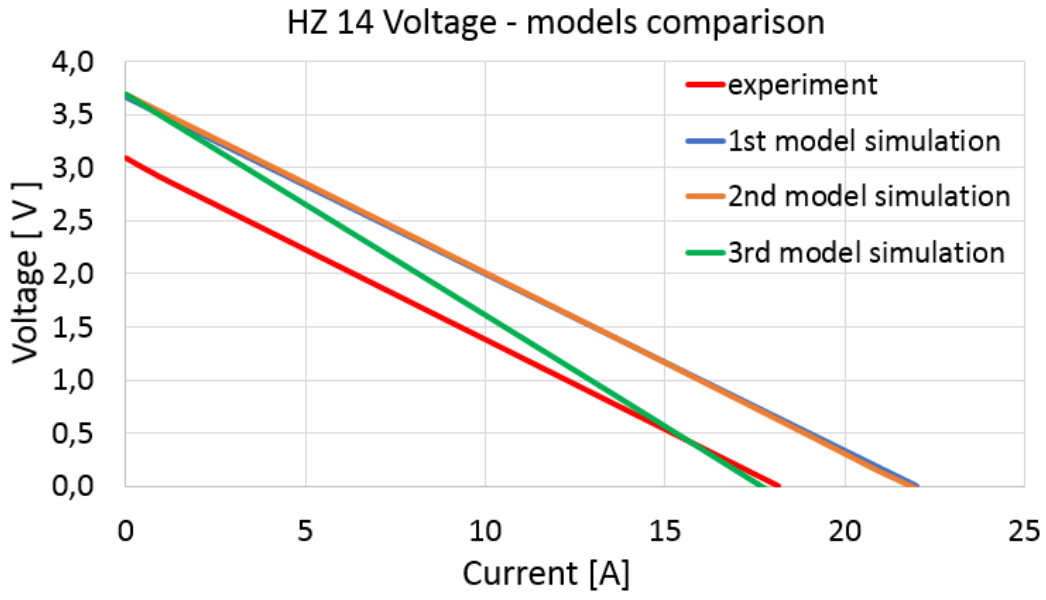

Figure 4.10: Models comparison, voltage curve performance compared with experiment.

One of the most important observation can be seen in the figure 4.10, where the voltage curves for three models simulation and experiment are plotted. One can observe that for the 1st and 2nd model the slope is only a litlle bit more mild than for experiment, but for the 3rd model the slope is much more sharp. This figure can suggest that on the one hand the contact resistant value set is not precise enough and should be presented in the form of some function and on the other hand the OCV value for all presented models is too high. This can be an effect of too optimistic Seebeck coefficient values presented in literature [8].

4.4 Full model - analysis

To analyze the model in more detail few more graphics extracted from the numeric analysis will be discussed. First of all, the voltage distribution in the domain is presented in figures 4.11 under open circle voltage and 4.11 under matched load. The unit of voltage range presented at the right side of the graphics is Volt.

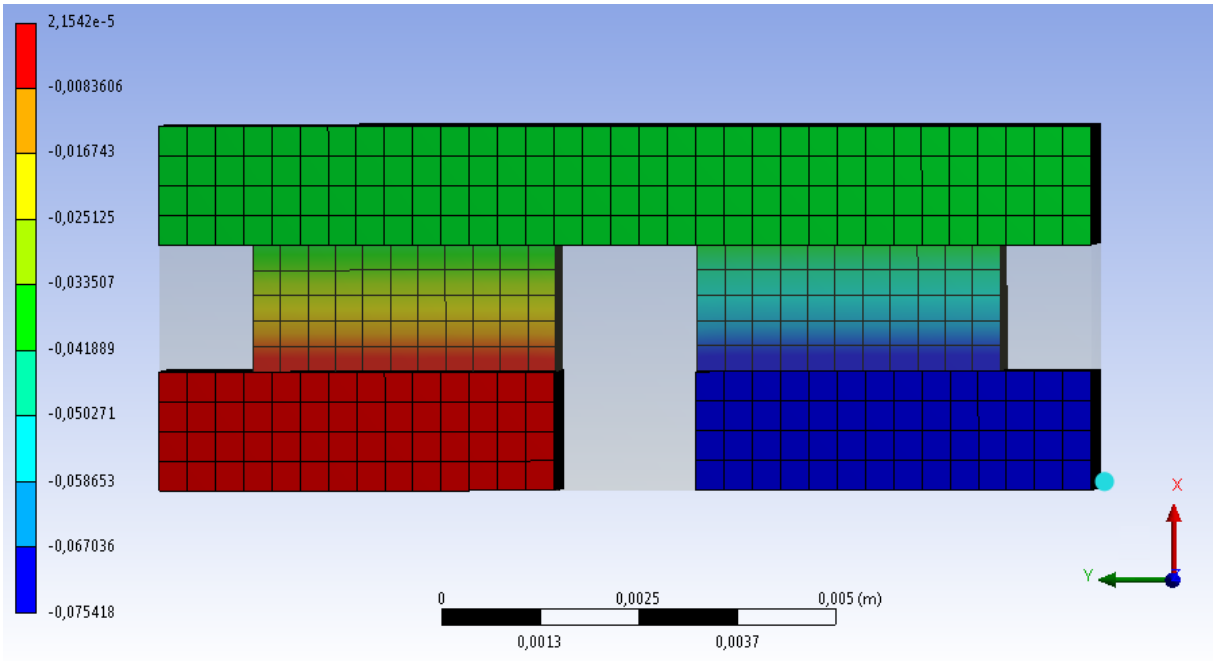

Figure 4.11: Voltage distribution in thermocouple, under open circle voltage, I = 0 A.

As it is known from the basics of physics the current flow generates Joule heat what is another source of losses. This component should be also included in TEG modeling. On the plot 4.13 the Joule heat generation rate in one thermocouple versus current density is presented. Obviously, the heat rate is increasing when the current value rises. Joule heat generation rate is reverse - proportional to material electric conductivity. Thus, as it can be seen in figure 4.14, here the unit is W/m^3. Joule heat generation rate in copper conductors is negligible in comparison to one in legs, composed from thermoelectric material.

In the figures 4.16 and 4.15 the temperature distribution(presented in Celsium degrees) of a single thermoelement and thermoelement with eggcrate under open circle voltage. It can be seen that on the

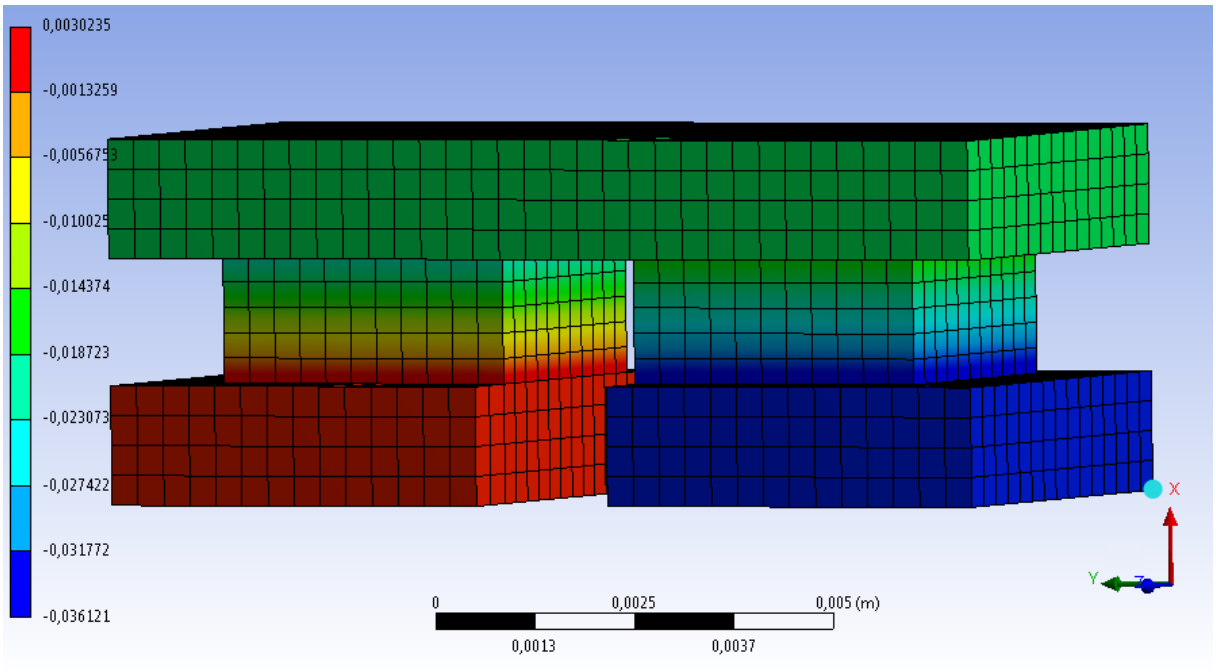

Figure 4.12: Voltage distribution in thermocouple, under matched load, I = 9 A.

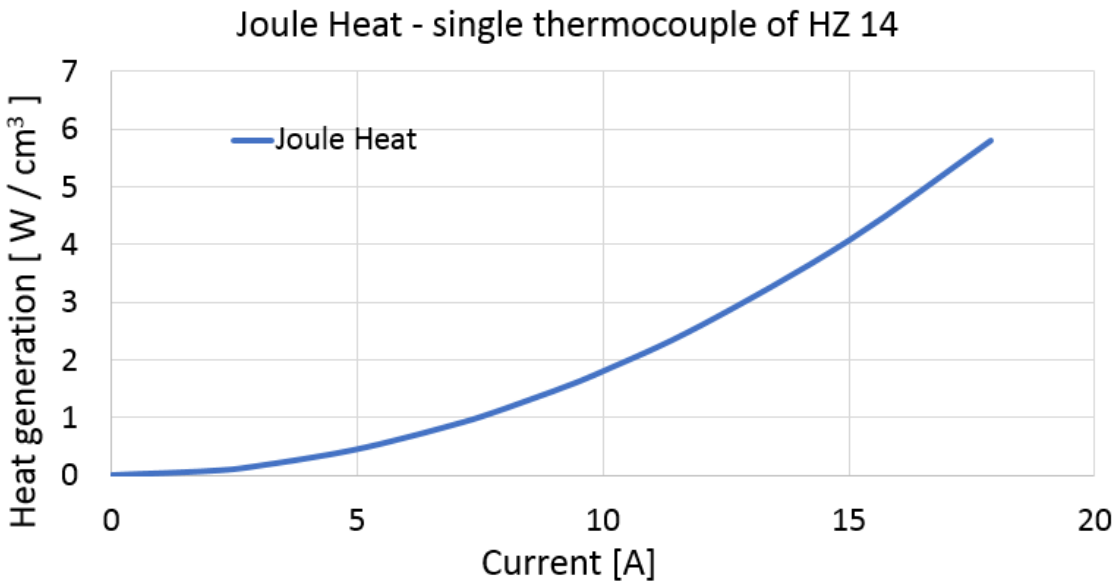

Figure 4.13: Joule Heat rate versus current density.

whole thickness of copper connectors the temperature is almost the same, which is the result of high thermal conductivity. All the temperature gradient is present in thermocouples legs and in eggcrate. The height of thermocouples legs is 1.6 mm and the temperature difference between its endings is almost 200 Celsium degrees, giving a huge temperature gradient. That is why the thermocouple legs should be characterized by high thermal durability to endure extreme working conditions.

The performance of the abovementioned graphics confirms that the simulation output generated by the model gives physical results, so it can be used for further analysis, like parametric studies.

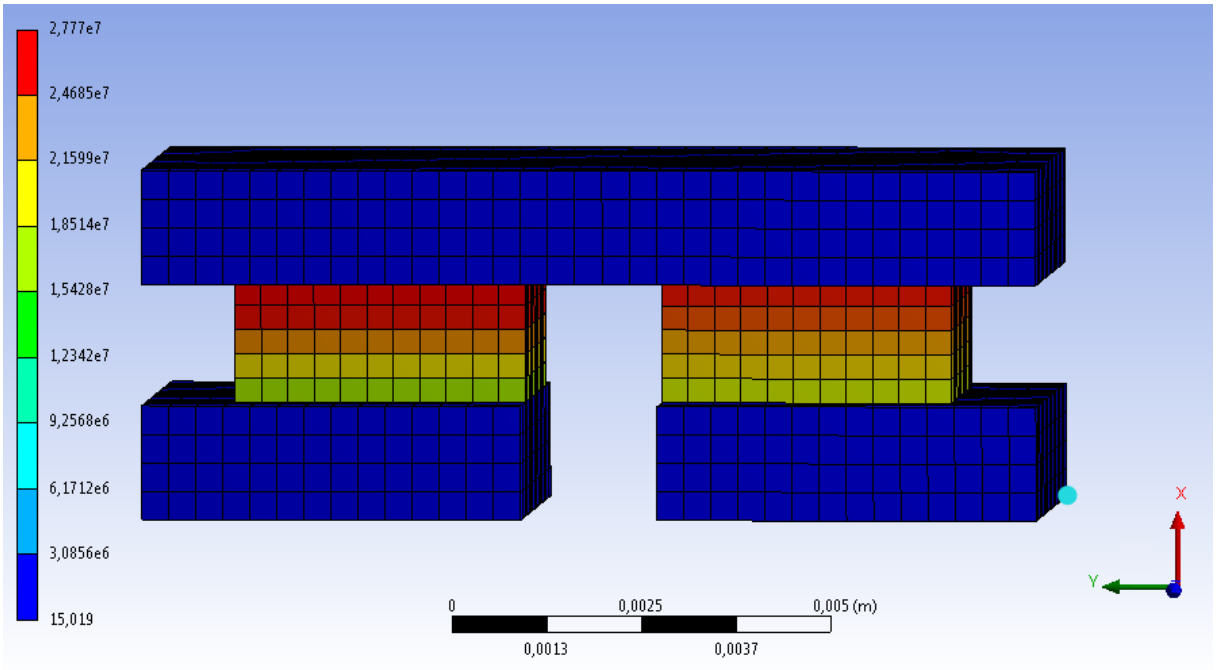

Figure 4.14: Joule Heat rate in thermocouple, under current = 18 A.

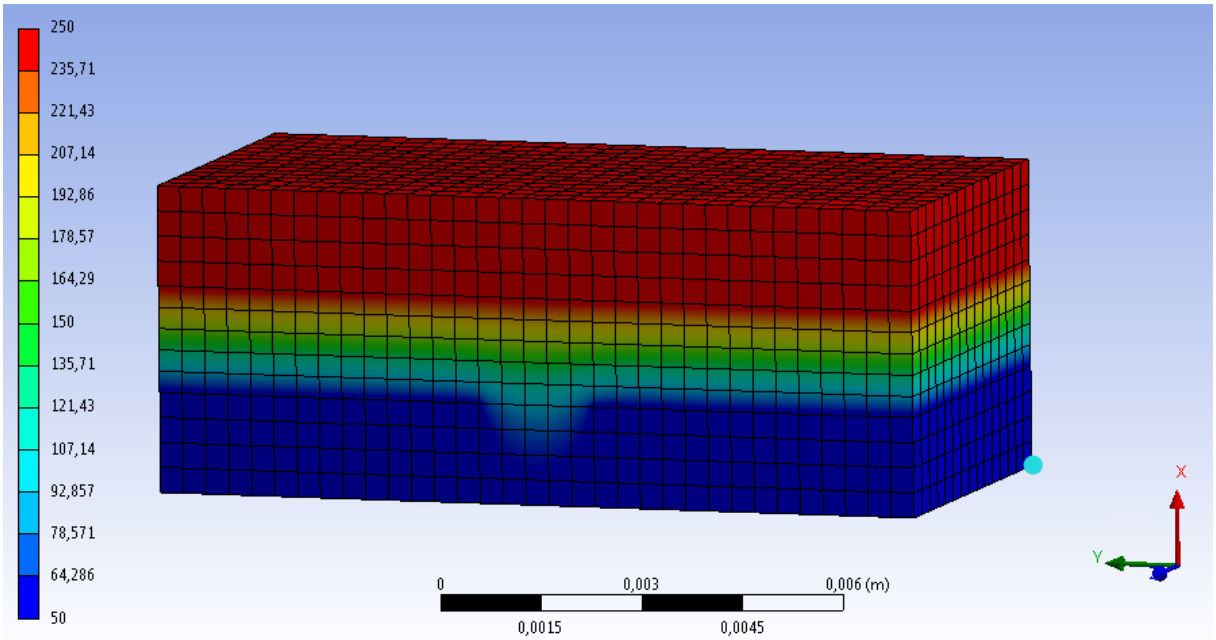

Figure 4.15: Temperature distribution - full thermocouple element.

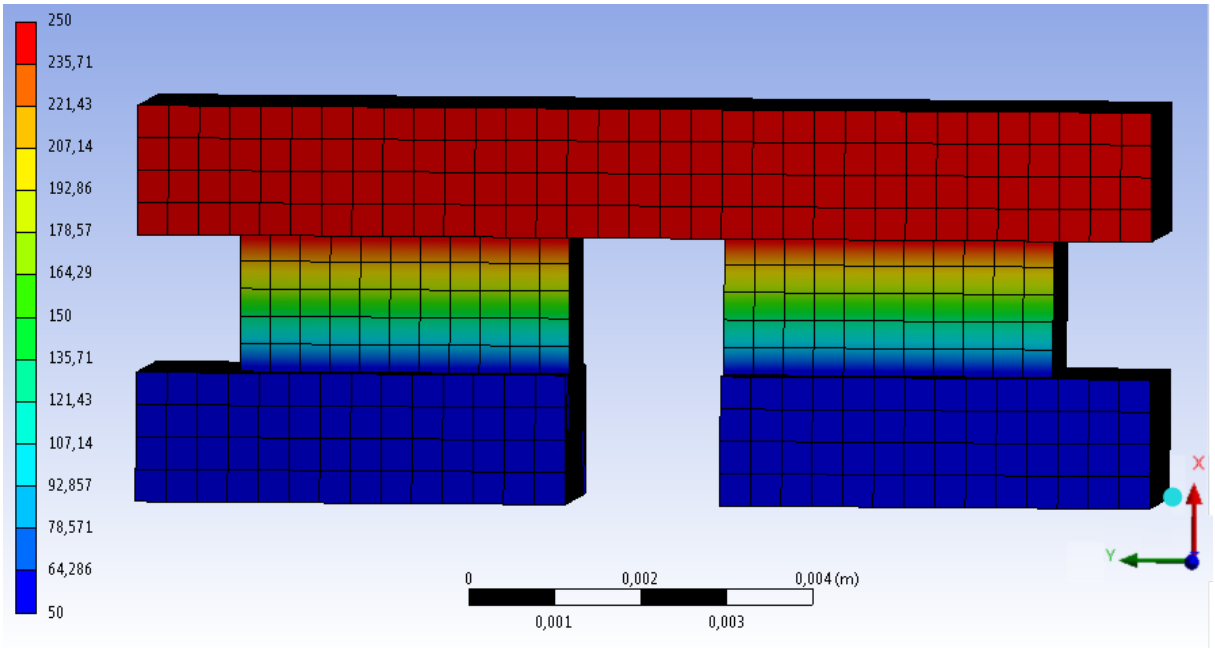

Figure 4.16: Temperature distribution - only thermocouple.

4.5 Parametric study

As the simulation results were considered as the correct mapping of the real HZ-14 thermoelectric generator, a little parametric study was performed. The model was tested for different temperature conditions. In vehicles, exhaust gas temperature depends on driving conditions and it is changing continuously. Thus, it was chosen as the most important external parameter, affecting TEGs operation. In the figures 4.18 the module power was tested for four different cold junction temperatures (T_c) and few other hot junction temperatures ranged from 160 ^{o} C to 360 ^{o} C. The performance of the module was tested for a matched load (I = 9 A). The obtained results were compared with experimental data for the same TEG module [16].

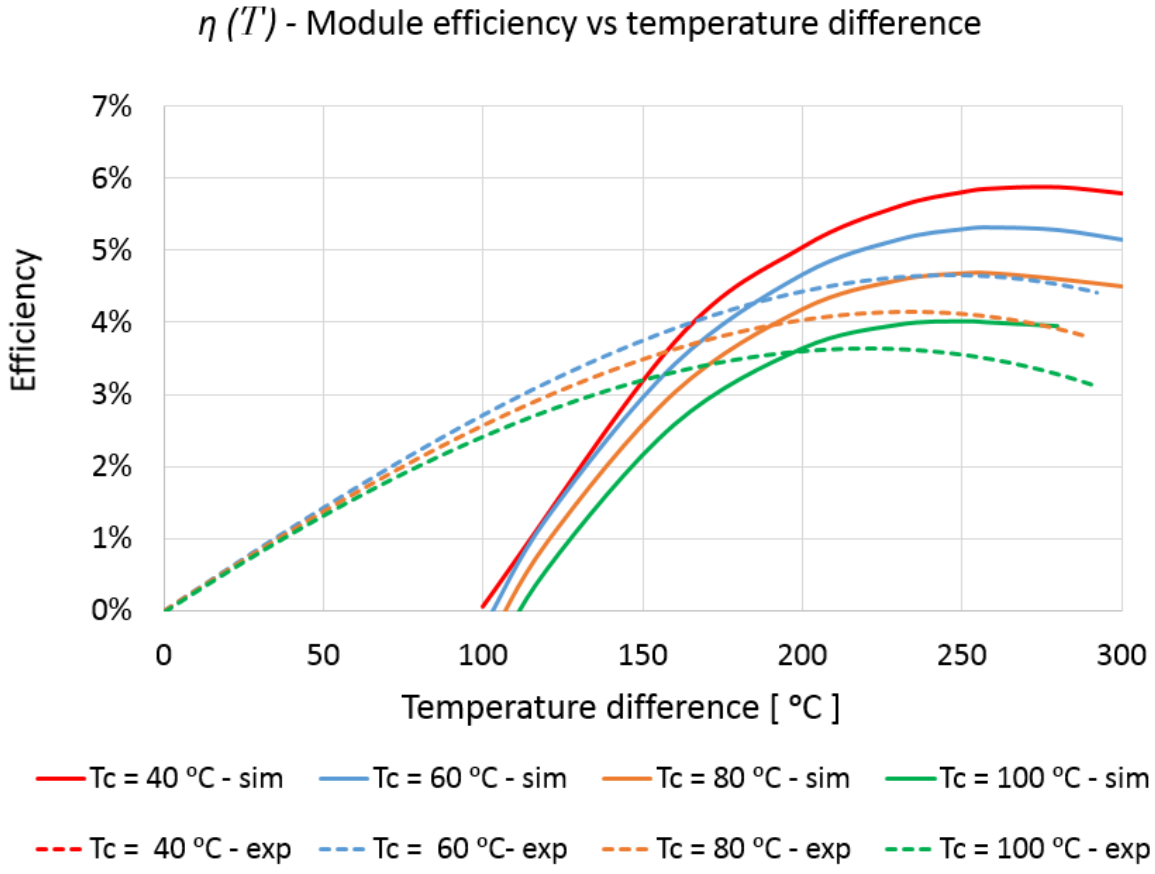

Figure 4.17: Model efficiency at matched load versus temperature, compared with experiment.

As can be seen, for efficiency curves the results generated by the model do not simulate the TEG module efficiency accurately. This discrepancy may be a consequence of assumed calculation methodology (described in section 4.3), which does not take into account all the heat phenomenons taking place in a real module.

The module power simulation results versus temperature difference between hot and cold sides predict power behaviour in a satisfactory way, expecially when temperature difference between hot and cold junction is above 160 ^{o} C. For lower temperature difference, the simulation results are incorrect. The similar discrepancy is visible in the figure 4.19. It can be expected, that the values for material properties

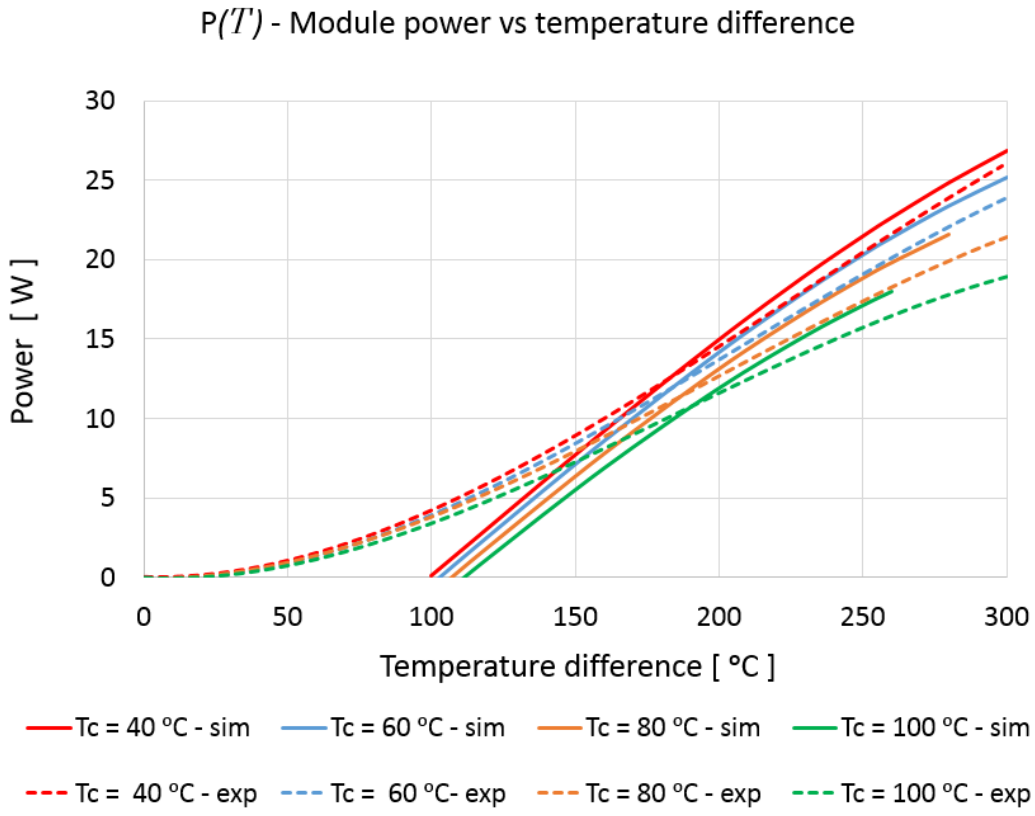

Figure 4.18: Model power at matched load versus temperature, compared with experiment.

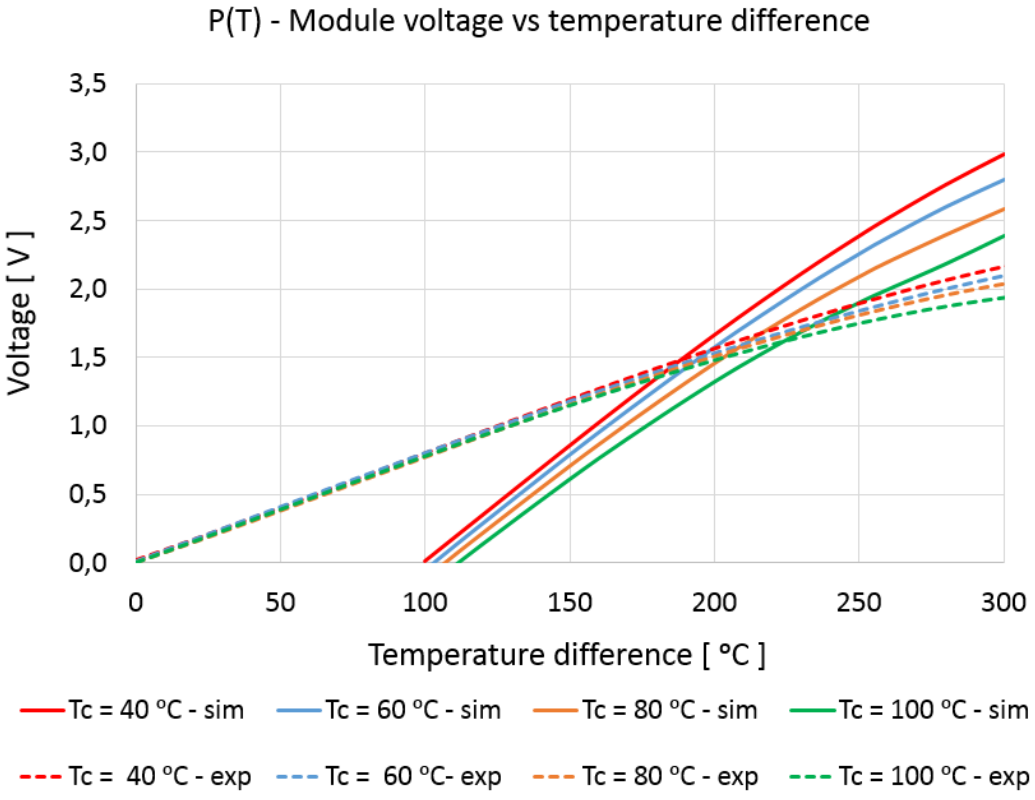

Figure 4.19: Model voltage at matched load versus temperature, compared with experiment.

or contact resistances should be examined in a more detailed way or there is more phenomenon to capture in the simulation of TEGs. thus, the next step of the research should be to establish a proper nonlinear relation for contact resistances.

Another important factor which could make an unfavorable impact on the model results is the fact, that data used for material properties were available in the temperature range between 50 - 250 ^{o} C. Thus, for the parametric study the material characteristics were extrapolated to the temperature value necessary to build above-attached plots. Moreover, it should be taken into account that the mesh in the model is coarse, because of the ANSYS student license limits.

All things considered, all the abovementioned factors affects the accuracy of the model, but the most important factor is contact resistance. On the figures below 4.20, 4.21, 4.22 the efficiency, power and voltage curves for the second model(without contact resistance apllied) versus experiment results are presented. It can be clearly seen that the curves shape seems to have more realistic shape than for the model with contact resistance. Although the fact that the values are overestimated significantly the shapes seems to be more ”physical”. Thus, one of the important theis outcome is that the contact resistance phenomenon should be investigated more carefully versus temperature. The legs and connectors are made from different materials with different microstructure and thermal expansion coefficient, so as it is presented in the thesis the value can vary significantly with operating temperature.

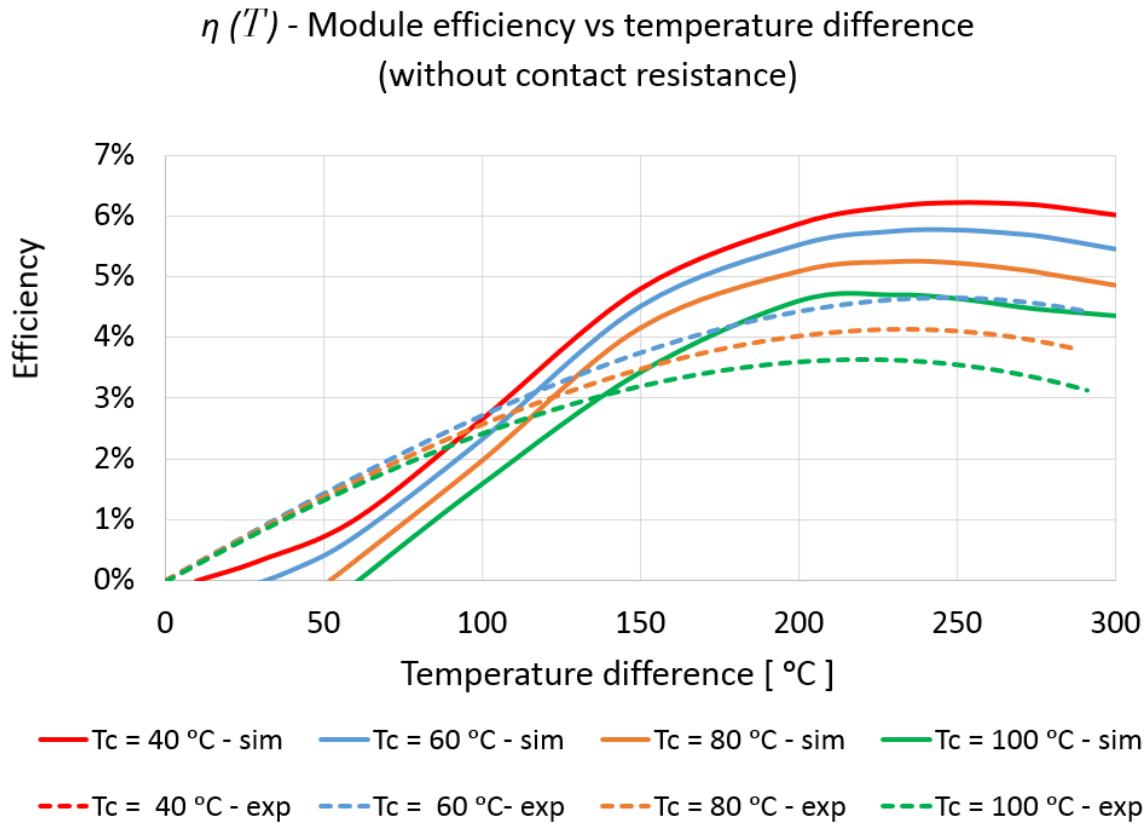

Figure 4.20: Model (without contact resistance applied) efficiency at matched load versus temperature, compared with experiment.

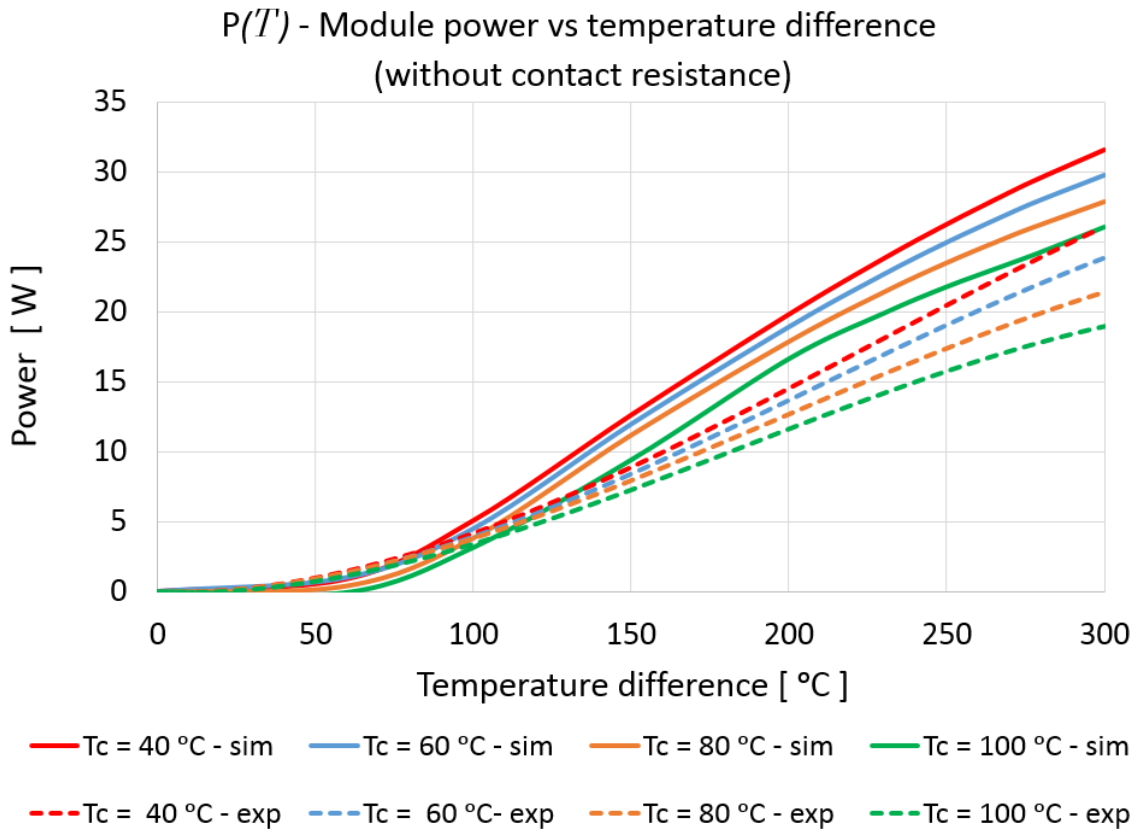

Figure 4.21: Model (without contact resistance applied) power at matched load versus temperature, compared with experiment.

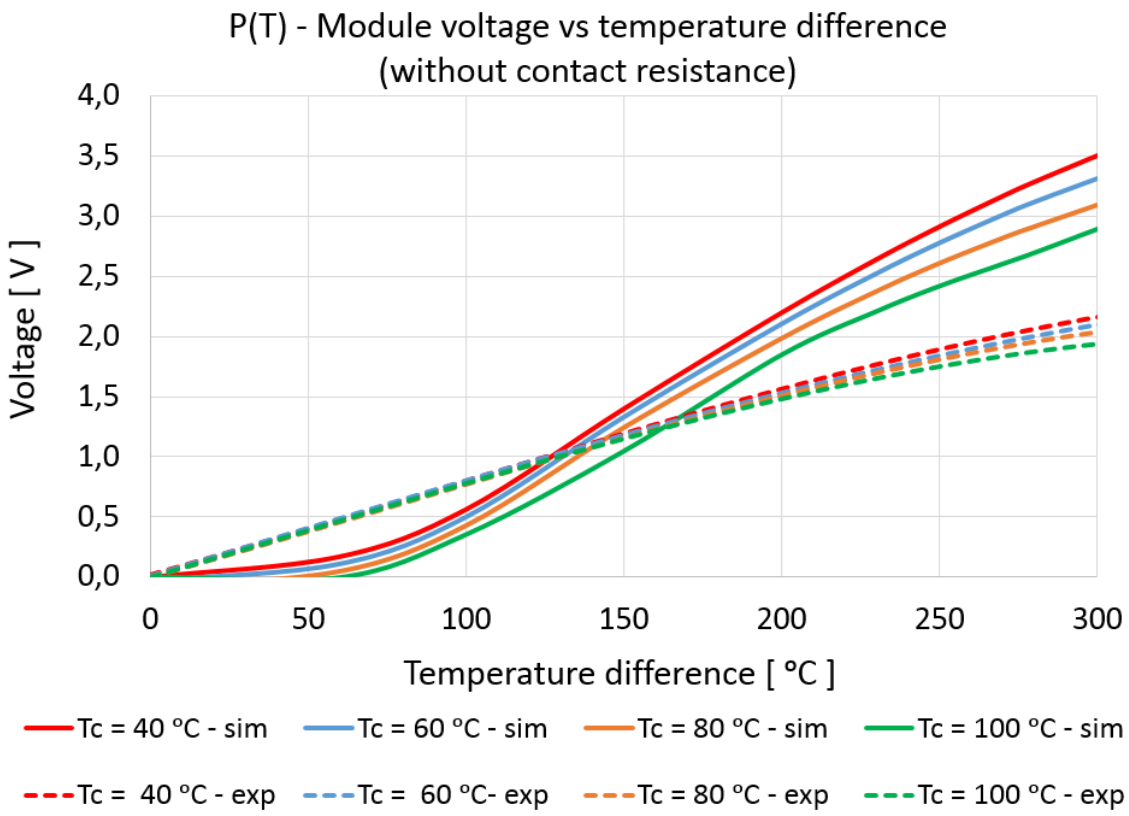

Figure 4.22: Model (without contact resistance applied) voltage at matched load versus temperature, compared with experiment.

Chapter 5

Conclusions

5.1 Achievements

The goal of the thesis was to proposed a benchmark approach for 3-D modeling of thermoelectric generator using Thermal-Electric module in ANSYS workbench. The starting point for model development was a simple model with constant parameters in order to check if the simplest solution has an acceptable level of error. However in order to accurately predict thermoelectric module performance there was a need to capture more physical phenomena like non-linear temperature-dependent behaviour of material properties and contact resistances. This helped to significantly improve the model to the level of acceptable utility.

From the results it can be observed that incorporation of temperature-dependant material properties does not significantly improves the result of the simulation, but it complicates the model implementation and prolongs the numerical calculation. The fact is that, contact resistances play a significant role in model performance. In this research only electrical contact resistances between legs and conectors were included, but it could be beneficial to include also thermal resistances between components. Going even deeper, the contact resistances should be also implemented as the temperature dependent functions. All in all, the results are satisfactory but there are still a few doubts regarding applied metodology. More details regarding future plans are mentioned in section 5.2. From the perspective of implementation of TEGs in hybrid vehicles, the conversion efficiency level of is still very low and the economic profitability doubtfull. As it was presented in parametric study the maximum available efficiency is around 5 % what is still low. As it was shown in the result analysis, all the limits lie in material properties. Now, the research should focus on minimization of the negative effects of contact region between thermocouple components.

Moreover, the outcome of the thesis confirms that Thermal-Electric module in ANSYS Workbench is an efficient, convenient and user-friendly environment to perform analysis dedicated for thermoelectric generator. The in-build submodules provide the easiness of implementing physics, boundary conditions, material properties and etc. Thanks to that, the numerical models elaboration is much faster and efficient than it would be with the help of scripting languages like C++, Python or even MATLAB. Moreover, the

multiphysics packages allows the user to incorporate the models like this presented in the thesis into more complicated model-assembly in coupling simulations of few different devices.

5.2 Future Work

During the process of thesis development appeared a few ideas on how to improve the modeling of thermoelectric generators. As it was presented in the thesis, extremely important factors on TEG modeling are contact resistance. Thus, this phenomenon should be accurately examined. All the contacts between each element should be measured, taking into consideration either electric or thermal contact resistances. Moreover, in my opinion, based on the thesis outcomes, the contact resistances should also be examined in relation to temperature changes, which could be a key factor for accurate model development. Another important step in further model development is the elaboration of the extended mathematical model for the complete HZ-14 module. This step would require building geometry of all the device components, extend the existing mathematical model, and define more practical boundary conditions. This approach would help us to capture all the thermal phenomena occurring in the module when operating and additionally capture all the ohmic losses appearing on interconnectors. All things considered, the presented topic is very interesting and the models should be improved because it is still a lot of knowledge to explore within the thermoelectric generators.

References

[1] L. Arnaud, G. Ludovic, D. Mouad, H. Zaïdi, and V. Lemort. Comparison and impact of waste heat recovery technologies on passenger car fuel consumption in a normalized driving cycle. *Energies*, 7:5273–5290, 2014.

[2] BP. Bp energy outlook, February 2015. URL: https://www.bp.com/content/dam/bp/business-sites/en/global/corporate/pdfs/energy-economics/energy-outlook/bp-energy-outlook-2015.pdf - Internet access on 23-03-2020.

[3] S. Kim, S. Park, S. Kim, and S. H. Rhi. A thermoelectric generator using engine coolant for light-duty internal combustion engine-powered vehicles. *J. Electron. Mater*, 40:812–816, 2011.

[4] B. Orr, A. Akbarzadeh, M. Mochizuki, and R. Singh. A review of car waste heat recovery systems utilising thermoelectric generators and heat pipes. *Applied Thermal Engineering*, 101:490–495, May 2016.

[5] D. Champier. Thermoelectric generators: A review of applications. *Energy Conversion and Management*, 140:167–181, 2017.

[6] G. P. Meisner. Thermoelectric generator development for automotive waste heat recovery. In *16th Directions in Engine Efficiency and Emissions Research (DEER) Conference*, Detroit, Michigan, September 2010. General Motors Global Research and Development.

[7] T. D. Deng, S. Chen, and N. Tong. Thermal optimization of the heat exchanger in an automotive exhaust-based thermoelectric generator. *Journal of Electronic Materials*, 42:1634–1640, 2013.

[8] T. Zhang. New thinking on modeling of thermoelectric devices. *Applied Energy*, 168:65–74, Feb. 2016.

[9] A. Abdelkefi, A. Alothman, and M. R. Hajj. Performance analysis and validation of thermoelectric energy harvesters. *Smart Materials and Structures*, 22:095014, 2013. doi: 10.1088/0964-1726/22/9/095014.

[10] Z. Niu, S. Yu, H. Diao, Q. Li, K. Jiao, Q. Du, H. Tian, and G. Shu. Elucidating modeling aspects of thermoelectric generator. *International Journal of Heat and Mass Transfery*, 85:12–32, 2015.

[11] A. Massaguer, E. Massaguer, M. Comamala, T. Pujol, J. González, M. Cardenas, D. Carbonell, and A. Bueno. A method to assess the fuel economy of automotive thermoelectric generators. *Applied Energy*, 222:42–58, 2018.

[12] S. Vale, L. Heber, P. Coelho, and C. Silva. Parametric study of a thermoelectric generator system for exhaust gas energy recovery in diesel road freight transportation. *Energy Conversion and Management*, 133:167–177, 2017.

[13] J. H. Meng, X. X. Zhang, and X. D. Wang. Dynamic response characteristics of thermoelectric generator predicted by a three-dimensional heat-electricity coupled model. *Journal of Power Sources*, 245:262–269, 2013.

[14] Z. Niu, H. Diao, S. Yu, K. Jiao, Q. Du, and G. Shu. Investigation and design optimization of exhaust-based thermoelectric generator system for internal combustion engine. *Energy Conversion and Management*, 85:85–101, 2014.

[15] M. Chen, L. A. Rosendahl, and T. Condra. A three-dimensional numerical model of thermoelectric generators in fluid power systems. *International Journal of Heat and Mass Transfer*, 54:345–355, 2010.

[16] I. Hi-Z Technology. Hz-14 datasheet. http://www.hi-z.com//wp-content/uploads/2016/09/Hi-Z-Data-Sheet-HZ-14-1.pdf - Internet access on: 18-07-2020, .

[17] H. S. Lee. *Thermal Design: Heat Sinks, Thermoelectrics, Heat Pipes, Compact Heat Exchangers, and Solar Cells*. John Wiley and Sons Inc, 2011.

[18] W. Thomson. On the dynamical theory of heat. part v. thermo-electric currents. *Transactions of the Royal Society of Edinburgh*, 21:123–171, 1854.

[19] H. J. Goldsmid. *The Physics of Thermoelectric Energy Conversion*. Morgan and Claypool Publishers, 2017.

[20] E. E. Antonova and D. C. Looman. Finite elements for thermoelectric device analysis in ansys. In *ICT 2005. 24th International Conference on Thermoelectrics*, Clemson, SC, USA, June 2005. ANSYS Inc.

[21] A. S. Kushch, J. C. Bass, S. Ghamaty, N. B. Elsner, R. A. Bergstrand, D. Furrow, and M. Melvin. Thermoelectric development at hi-z technology. In *Proceedings ICT2001. 20 International Conference on Thermoelectrics*, Beijing, China, June 2001. Hi-Z Technology, Inc. PACCAR Technical Center.

[22] O. Hogblom and R. Andersson. Analysis of thermoelectric generator performance by use of simulations and experiments. *Journal of Electronic Materials*, 43:2247–2254, 2014.

[23] P. P. Silvester and R. L. Ferrari. *Finite Elements for Electrical Engineers*. Cambridge University Press, 1996.

[24] P. Kohnke. *Theory Reference*. ANSYS Inc., Southpointe, Technology Drive, Canonsburg, PA 15317, USA, 5.6 edition, 1999.

[25] I. Hi-Z Technology. Hi-z technology performance calculator. https://hi-z.com/performance-calculator - Internet access on: 18-07-2020, .